# Competitive Metabolite Profiling of Natural Products based on Syringolin A probe.

**Doctoral thesis for obtaining the**

**Academic degree Doctor of**

**(Dr.rer.nat.)**

Submitted by

Pawar, Atul

at the

Universität Konstanz

Mathematisch-Naturwissenschaftliche Sektion

Fachbereich Chemie

Konstanz, 2020.

Date of the oral examination: 23/03/2021

1. Reviewer: Dr. Thomas Boettcher

2. Reviewer: Prof. Dr. Marcus Groettrup

# Acknowledgements

Firstly, I would like to thank my thesis advisor Dr. Thomas Boettcher. His office to me was always open for guidance, discussion and counsel. He consistently allowed this research to be my own work, and steered me in the proper direction when asked for.

I would like to thank Prof. Dr. Marcus Groettrup for his help during the research and insightful discussions about any subject matter discussed in the thesis. Furthermore, I appreciate the help from his lab, especially, Dr. Michael Basler and Gerardo Salinas for their help in providing help and research essential for this work.

Next, I would like to thanks my co-workers in the lab, Dr. David Szamosvári, Dr. Sina Rütschlin, Dr. Micheala Prothiwa, Lilian Penalvar, Magdalena Jancheva, Jacopo Meazza, Nhung Nguyen and Dr. Grazyna Durak for their company inside and outside of lab.

This research could not be possible without the support and help of Konstanz Research School Chemical biology (KoRS-CB), Fonds der Chemiche Industrie (FCI), SFB 969, and DFG. Their financial support for the idea behind this thesis was very much essential. Special thanks to Prof. Dr. Valentin Wittmann and Prof. Dr. Florian Stengel for support and help during thesis.

Lastly, I would like to express my gratitude for my parents, my brother, my sister-in-law for providing me with unwavering support and encouragement throughout my learning years. This thesis would not be accomplished without your support, thank you.

Sincerely,

Atul Pawar.

# Index of abbreviations

| | |
|---|---|
| ABP | Activity-based probe |
| ABPP | Activity based protein profiling |
| abs. | Absolute |
| APS | Ammonium peroxydisulfate |
| BSA | Bovine serum albumin |
| CC | Click Chemistry |
| conc. | Concentration |
| COSY | Correlation spectroscopy |
| d | Doublet |
| Da | dalton (g/mol) |
| deion | Deionized |
| DMSO | Dimethylsulfoxide |
| USFDA | U.S. Food and Drug Administration |
| GlbA | Glidobactin A |
| HPLC | High-performance liquid chromatography |
| Hz | Hertz |
| m | Multiplet |
| M | Molarity (mol/L) |
| MS | mass spectroscopy |
| NMR | Nuclear magnetic resonance |
| Ntn | N-terminal nucleophilic |
| ppm | parts per million |
| Pss | Pseudomonas syringae pv. syringae |
| q | Quartet |
| quin | Quintet |
| Rh-Syl | Rhodamine tagged Syringolin A |
| rpm | Revolutions per minute |
| s | Singlet |
| SDS | Sodium dodecyl sulfate |
| SDS-PAGE | Sodium dodecyl sulfate-polyacrylamide gel electrophoresis |
| SOB | Super Optimal Broth |
| SRM | Syringomycin media |
| SylA | Syringolin A |
| t | Triplet |
| TCEP | Tris(2-carboxyethyl)phosphine |
| TEMED | N,N,N’,N’-tetramethylethylenediamine |
| SylA | Syringolin A |
| SylP | Syringolin A probe |
| GlbA | Glidobactin A |
| LumA | Luminmycin A |
| GlbC | Glidobactin C |

# Table of Contents

# Summary

Although the conventional methods for inhibitor identification in drug discovery have yielded good results with respect to natural products as medicinal drugs, these methods are usually time-consuming, resource intensive and limited in scope. Within the scope of this thesis, the plan was to identify and study new bioactive natural products, which have so far remained undiscovered in traditional screening strategies. In this thesis, I present the development of a method, using competitive natural product as a probe labelling strategy that can utilize active sites of the target protein directly, rather than using a shotgun approach. This novel method is named “Competitive metabolite profiling of natural products”. This strategy uses a highly specific metabolite probe synthesized from natural product to competitively inhibit target of interest. The probe mainly consists of an alkyne moiety and electrophilic group for labelling and targeting respectively. This probe is then used to label proteolytic subunits of human and mouse proteasomes competitively, with crude extracts containing potential inhibitors of proteasome. Using activity guided detection and isolation, three inhibitors were successfully isolated, subsequently analytical methods were applied to characterize them. Cell-based assays and subunit specific assays allowed elucidation of a surprising subunit specificity of one the inhibitors.

# Zusammenfassung

Obwohl die konventionellen Methoden zur Identifizierung von Inhibitoren in der Arzneimittelforschung gute Ergebnisse in Bezug auf Naturstoffe als Arzneimittel erzielt haben, sind diese Methoden in der Regel zeitaufwendig, ressourcenintensiv und in ihrem Umfang begrenzt. Im Rahmen dieser Arbeit war geplant, neue bioaktive Naturstoffe zu identifizieren und zu untersuchen, die in den traditionellen Screeningstrategien bisher unentdeckt geblieben sind. In dieser Arbeit stelle ich die Entwicklung einer Methode vor, bei der ein konkurrierendes Naturprodukt als Sondenmarkierungsstrategie verwendet wird, die aktive Stellen des Zielproteins direkt nutzen kann, anstatt einen Schrotflintenansatz zu verwenden. Diese neuartige Methode wird als "Competitive Metaboliten-Profiling von Naturstoffen" bezeichnet. Diese Strategie verwendet eine hochspezifische Metabolitensonde, die aus einem Naturprodukt synthetisiert wird, um das Ziel von Interesse konkurrierend zu hemmen. Die Sonde besteht hauptsächlich aus einer Alkin-Einheit und einer elektrophilen Gruppe zur Markierung bzw. zum Targeting. Diese Sonde wird dann verwendet, um proteolytische Untereinheiten von Human- und Maus-Proteasomen kompetitiv zu markieren, wobei Rohextrakte potentielle Inhibitoren des Proteasoms enthalten. Mit Hilfe von aktivitätsgeführter Detektion und Isolierung wurden drei Inhibitoren erfolgreich isoliert und anschließend mit analytischen Methoden charakterisiert. Zellbasierte Assays und Untereinheiten-spezifische Assays ermöglichten die Aufklärung einer überraschenden Untereinheiten-Spezifität eines der Inhibitoren.

# Introduction

Since prehistoric times, nature, environment and the advancement of culture has stimulated humans to continuously probe, test and explore the wide range of natural phenomena. Human activity often reveals impressive and ingenious approaches to these natural phenomena, exploration of which has a continuous and profound impact on human existence. Yet, concurrent to humans becoming more proficient at utilizing resources in their vicinity, they have also, in many cases, come closer to recognizing their own limitations in fully understanding scientific phenomena as well as understanding the consequences of human activity on nature. Many would agree that the relationship between humanity and natural resources over the years has not only reaffirmed their value, but have also led to a greater collective consciousness on how to access these vast arrays of resources more efficiently to further human civilization.

Microorganisms produce a multitude of structurally diverse secondary metabolites, some of which can be adapted for medicinal, veterinary or environmental applications. These small molecules may show antibiotic, anti-tumor or anti-inflammatory responses. The discovery of penicillin as an antibacterial agent in 1929 revolutionized medicine and stimulated extensive screening of microbes, aimed to identify more antibiotics in the following years [1]. In the 1960s, the development of potential anti-cancer agents was promoted based on the same strategy as the antibiotic research, and yielded drugs which are still in use today.

In general, bioactive small molecules termed natural products are still an important source for lead molecules, active pharmaceutical ingredients as well as for drug discovery and development. This emphasizes the dependence of synthetic and medical advances on fundamental biological research. For example, half of the approved small molecules applied in oncology in the last decades are natural products or substances which are directly derived from them. Libraries of synthetic compounds obtained via combinatorial chemistry are generally of low biological relevance, and just a few compounds were proven suitable for further drug development. In contrast to these synthetic compounds, natural products are often synthesized for wide variety of functions both inside and outside of microorganisms and have already undergone natural selection and evolutionary pressure for favorable interactions with essential proteins, target enzymes or other components of cellular machinery. Microorganisms

also express a variety of metabolites which evolved for targeting specific functions for survival. Thus, these molecules serve as model compounds with novel molecular structures and need little modifications for application as pharmaceuticals. Improvement of the medicinal effects of natural products can be achieved, for example, by optimization of synthesis, yielding more specific agents. In addition to the use in clinical studies, natural products are of great interest for revealing and understanding intracellular mechanisms, immune response and disease mechanisms in basic cellular biology.

## Natural products

Natural products are myriad, ubiquitous, and diversified assortment of organic compounds which rarely participate in direct growth, development, and internal economy of the producing organism, these organic compounds are called secondary metabolites. In contract, the primary metabolites such as amino acids, nucleotides, carbohydrates are metabolically essential and ubiquitous in all life forms. Historically, chemists have been proactive in investigating novel natural products; studies of natural products demanded the development of separation techniques, analytical approaches including spectroscopy and structure elucidation methodology. These combined techniques now constitute foundations of contemporary organic chemistry. Discovery of antibacterial crude extract “penicillin G” by Fleming in 1928, further purification and clinical research by Chain et.al. In early 1940s catapulted the natural product based drug discovery research. Large industries and research groups around the word started maintaining microorganism collection for natural product discovery. This natural product discovery included examples like streptomycin, chloramphenicol, and tetracycline. This natural product based compounds or derivatives of them are still in clinical usage as drugs till date. Since 1981 till 2019, out of 185 small molecules approved for treatment of cancer, 62 or 33% are based on natural products or derivatives of them as shown in **Figure 1**.[1]

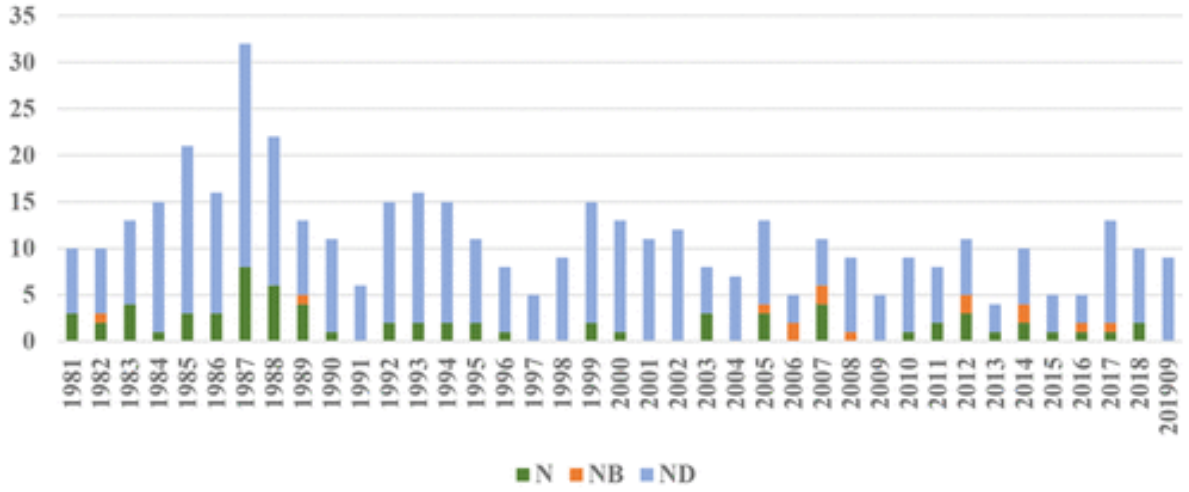


**Figure 1**: FDA approved drugs, data from 1981-2019, N: Natural product, NB: natural product botanical mixtures, ND: natural product derivatives.[1]

## Proteasome

Eukaryotic proteasome is an important protein regulatory and proteolytic complex that is responsible for protein homeostasis independently of lysosomal protein degradation machinery. It plays an important and central role in many of the basic cellular processes, including immune response, cell cycle, apoptosis and signaling pathways. The Proteasome based ubiquitin degradation pathway is one of the main pathways for protein degradation of key signaling proteins and abnormal or misfolded proteins in eukaryotic cells.

Four types of the proteasome are found in eukaryotes, constitutive proteasome, immunoproteasome, thymoproteasome, and mammalian testis-specific proteasome. The constitutive proteasome is well characterized, organized protein complex with sedimentation coefficient of 20S and molecular mass of 750 kDa. The immunoproteasome is structurally similar to the constitutive proteasome with β1, β2 and β5 subunits replaced with β1i, β2i and β5i, respectively due to exposure of cells to interferon-γ. The immunoproteasome is responsible for preparing peptide epitopes for cytotoxic T lymphocytes and important role in MHC class 1-restricted antigen-processing pathway and cell-mediated immunity. The thymoproteasome is expressed in cortical thymic epithelial cells with a novel catalytic subunit called β5t, its deficiency in mice displays defects in $CD8^+$ T cells.[2]

The 26S proteasome is made up of the 20S catalytic core particle and one or two 19S regulatory particles. These 19S regulatory particles identify ubiquitinated proteins, cleave the polyubiquitin chains off, unfold the protein and translocate it into the 20S proteasome where the ATP-dependent proteolysis takes place. The 20S catalytic core is made up of four stacked rings with a α7β7β7α7 barrel-shaped arrangement of subunits, whereby only the β1, β2 and β5 subunits harbor proteolytic sites. The proteasome β subunits belong to the family of the N-terminal nucleophilic (Ntn) hydrolases whose active sites consist of N-terminal threonine residues facing the inner cavity. Each of these subunits harbors different activities: β5 a chymotrypsin-like activity, β2 a trypsin-like one and β1 a caspase-like one. These constitutive catalytic subunits are replaced by LMP2 (β1i), MECL (β2i) and LMP7 (β5i) under the influence of cytokines such as IFN-γ resulting in the expression of the immunoproteasome in cells and tissues of the immune system. These differing proteolytic subunits cause changed substrate specificity.[3]

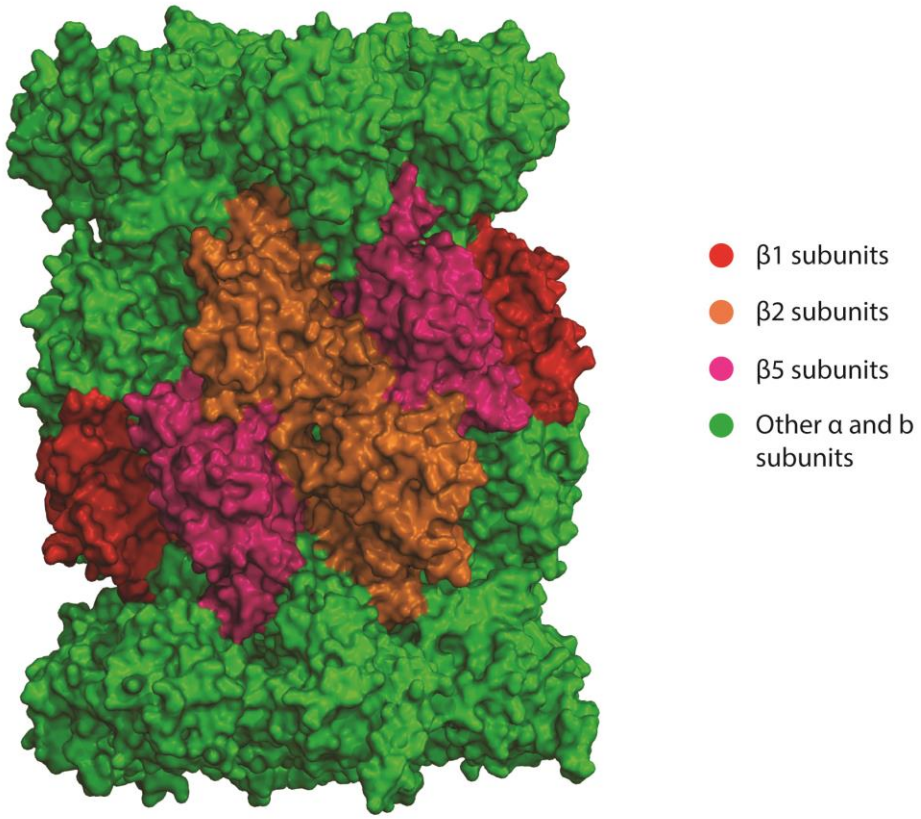


**Figure 2**: X-ray model structure of the 20S core Human constitutive proteasome, color coded subunits (PDB id: 5LE5).

## Proteasome inhibitors from natural sources

Proteasome inhibitors are structurally varied and diverse, but can be divided into 2 classes, reversible and non-reversible inhibitors. There are 5 major structural classes of naturally occurring proteasome inhibitors: aldehydes, β-lactones, epoxyketones, syrbactins, and cyclic peptides.[4]

Peptide aldehydes, examples are tyropeptin A and fellutamide B as shown in **Figure** 3(A). They are potent inhibitors of proteasome by forming a hemiacetal with hydroxyl of active site threonine. Although, their effectiveness is reduced as aldehydes are oxidized rapidly in vivo and do not present system wide inhibition activity when studied in mice.[5,6]

β-lactones, examples are omuralide and belactosin A as shown in **Figure 3B**. These are nonpeptide natural products more specific than aldehyder based inhibitor but are known to have effect on serine proteases (cathepsin A and mtLon). Salinosporomide A is a natural product recently discovered from *Salinispora tropica.* Mechanism of action of β-lactones is by esterifying the hydroxyl catalytic threonine.β-lactones present a disadvantage that the adducts are slowly hydrolyzed by water, making the proteasome active again.[7,8]

Epoxyketones, examples are epoxomicin and eponemycin as shown in **Figure 3C**. These are the most specific and potent proteasome inhibitors known natural products as no off target binding of these inhibitors are yet found. The crystal structure with yeast 20S proteasome offers insight into the specificity of these inhibitors as six-membered morpholine ring is formed with N-terminal threonine and epoxyketone moiety of the inhibitor. Lot of epoxyketones have been synthesized and studies for site specific inhibitors and activity based probes for profiling.[9,10]

Syrbactins, examples are syringolin A and glidobactin A as shown in **Figure 3D**. They consist of 12 membered lactam core attached to peptidyl tail region. The α,β-unsaturated amide in this lactam structure undergoes Michael-type 1,4-addition of the hydroxyl of the catalytic threonine to yield an irreversible and stable ether bond. These class of inhibitor have minimal off-target effects.[11–14]

Cyclic peptides, examples are TMC-95 A-D, scytonemides A and Argyrin A as shown in **Figure 3E**. These are novel cyclic tripeptides which are potent inhibitors of proteasome. Argyrin A was isolated from myxobacteria *Archangium gephyra* and TMC-95 A-D was isolated from *Apiospora montagnei Sacc*. TC 1093. Recently discovered scytonemides A and B were discovered from cyanobacterium *Scytonema hofmannii*. Binding mode of these cyclic peptide based inhibitors is not known as crystal structure has not been elucidated yet.[15,16]

## Inhibitor discovery with activity based protein profiling

Activity based protein profiling (ABPP) is function based proteomic methodology that uses active site directed, covalently binding electrophilic probes to target and label nucleophilic active sites of proteins which are similar in function and activity[17]. ABPP has generated invaluable insights in functional proteomics and discovery of novel functions of previously unknown proteins or enzymes. ABPP probes utilize a wide variety of scaffold including electrophile moieties, natural product inhibitors and synthetic structure based inhibitors. ABPP is widely used to isolate key enzymes of a particular class with help of a basic aspect of enzyme, the catalytic activity. Several different probes exist for different enzyme classes, including proteases, kinases, phosphatases, and oxidoreductases. Moreover, ABPP enables us to gain information about enzymes under physiological conditions. Activity based probes (ABPs) consists mainly of “warhead”, which could be an enzyme active site inhibitor or electrophilic moiety, a linker or spacer group and reporter tag for visualization or detection labeled protein.[18] In recent ABPP experiments, the reporter tag is often alkyne or azide functional group, due to their small size and relative low variance in cell permeability and inhibitor function. Such probes are often used in two-step protein labelling: initially ABPs are added to biological system *in vivo* for binding and consequently a reporter tag is attached such as a fluorophore containing moiety via biorthogonal conjugation such as modified Staudinger ligation and Huisgen 1,3–dipolar cycloaddition, collectively known as Click chemistry (CC).[19]

Recent research in chemical biology has seen increased interest in small molecule for engineering novel biological, inhibitor discovery, high throughput screening, using analytical platforms such as 1D-SDS-PAGE, LC-MS and more recently either with ABPP microarrays and Capillary electrophoresis coupled with Laser induced

fluorescence (CE-LIF).[20] ABPP can essentially answer three major questions in chemical biology landscape, comparative ABPP for target discovery, Competitive ABPP for inhibitor discovery and characterization of enzyme active sites.[21]

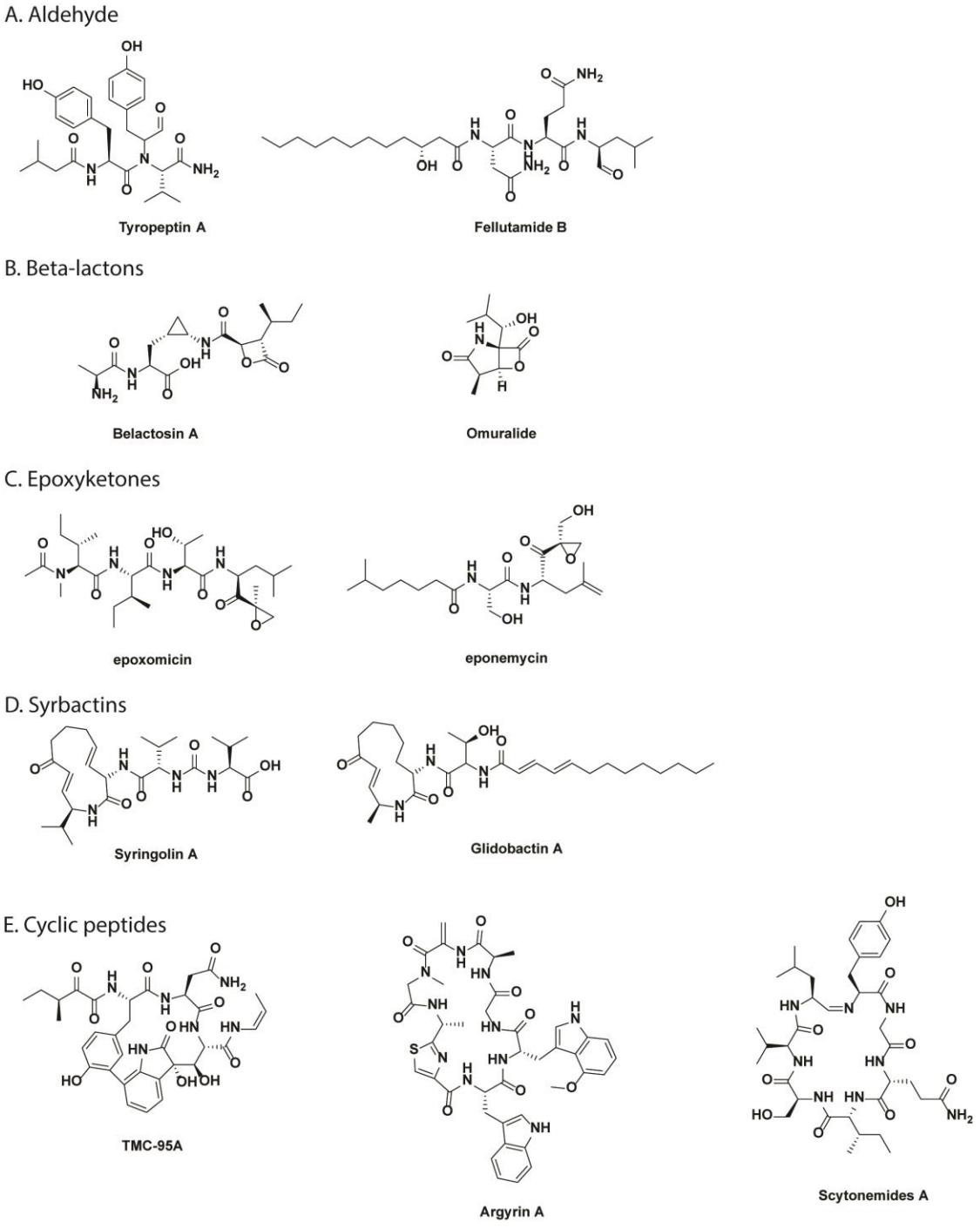


**Figure** 3: Five major structural classes of natural product inhibitors of proteasome. A: Aldehydes, B: Beta-lactons, C: Epoxyketone, D: Syrbactins and D: Cyclic peptides.

## Syrbactins biosynthesis

Phytopathogen names *Pseudomonas syringae*, produces a family virulence factor called Syringolins. These factors cause programmed cell death at the infection sites. Syringolin acts as a virulence factor by impairing the salicylic acid based host immunity, closure of stromata on leaves and proteasome inhibition.[13] These syringolins are biosynthesized by mixed nonribosomal peptide synthetase/polyketide synthase (NRPS/PKS) as shown in **Figure 4**.

The gene cluster comprises of 5 open reading frames (ORFs), named sylA, sylB, sylC, sylD, and sylE. The sylA ORF encodes a helix-turn-helix motif with a LuxR type DNA binding domain, which is primarily responsible for transcriptional regulator. sylB ORF functions as desaturator of 3,4-dehydrolysine residue. sylC and sylD are the NRPS and PKS modules in the gene cluster. Lastly, sylE encodes for major facilitator superfamily protein responsible for export of the syringolin A.[22]

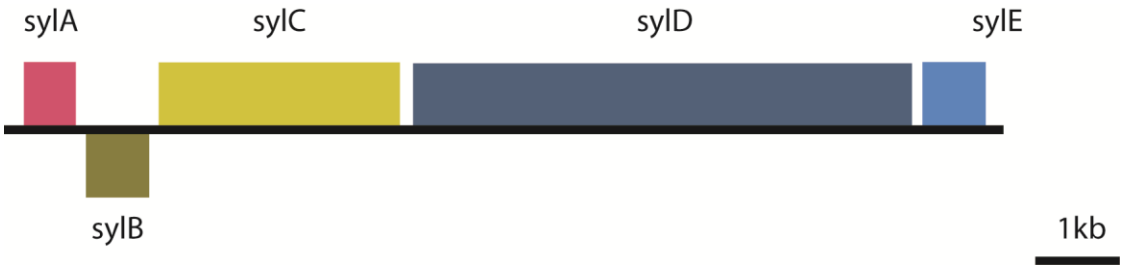


**Figure 4**: Illustration representing a part genome of *Pseudomonas syringae pv. syringae* B301D-R containing sylA to sylE genes.

## Aim and outline of thesis

Even though the conventional methods for inhibitor identification in drug discovery have yielded medically important drugs with respect to natural products, these methods are usually time and resource intensive along with being limited in scope. In this thesis, my aim was to identify and study new bioactive natural products, which have so far remained undiscovered in traditional screening strategies. This thesis describes the development of a method using natural product as a probe with competitive labelling strategy that can utilize active sites of the target protein directly rather than using a shotgun approach. This novel strategy was named as “Competitive metabolite profiling of natural products”. This strategy uses a highly specific metabolite probe synthesized from natural product to competitively inhibit target of interest. The probe mainly consists of an alkyne moiety and electrophilic group for labelling and targeting respectively. This probe was then used to label proteolytic subunits of human and mouse proteasomes competitively with crude extracts containing potential inhibitors of proteasome. Using activity guided detection and isolation procedures, I was able to isolate three inhibitors; further, using analytical methods were able to identify them. Cell-based assays and subunit specific assays were able to elucidate a surprising subunit specificity of one the inhibitors.

# Results: SDS-PAGE based activity guided inhibitor discovery

## Syringolin A production, isolation and, characterization

The first step for screening of new inhibitors of proteasome was to establish a natural product-based probe. The requirements for such a probe were, to be of natural origin, a non-reversible (covalent) inhibitor, a small molecule, easy to modify at non-essential moieties in the structure. Syringolin A met these requirements and was relatively easy to purify in quantities needed for chemical modification. Using a construct of Pseudomonas plasmid over expressing all the genes required for SylA production in *Pseudomonas syringae,* SylA was produced and secreted into the media by the bacteria within 10 days of incubation. The production of syringolin A was monitored with Analytical HPLC and HR-MS analysis. Series of purification steps from using XAD-16N beads, Preparative HPLC, until final semi-preparative HPLC purification. **Figure 5A** shows the preparative HPLC chromatogram of the final Syringolin A purification. Along with Syringolin A, minor quantities of Syringolin B - E were detected by HR-MS but were proven difficult to purify due their relatively poor separation with each other and poor overall yield. The characterization of Syringolin A was carried out using HR-MS and NMR analyses (**Figure 5B** and **Figure 26**).

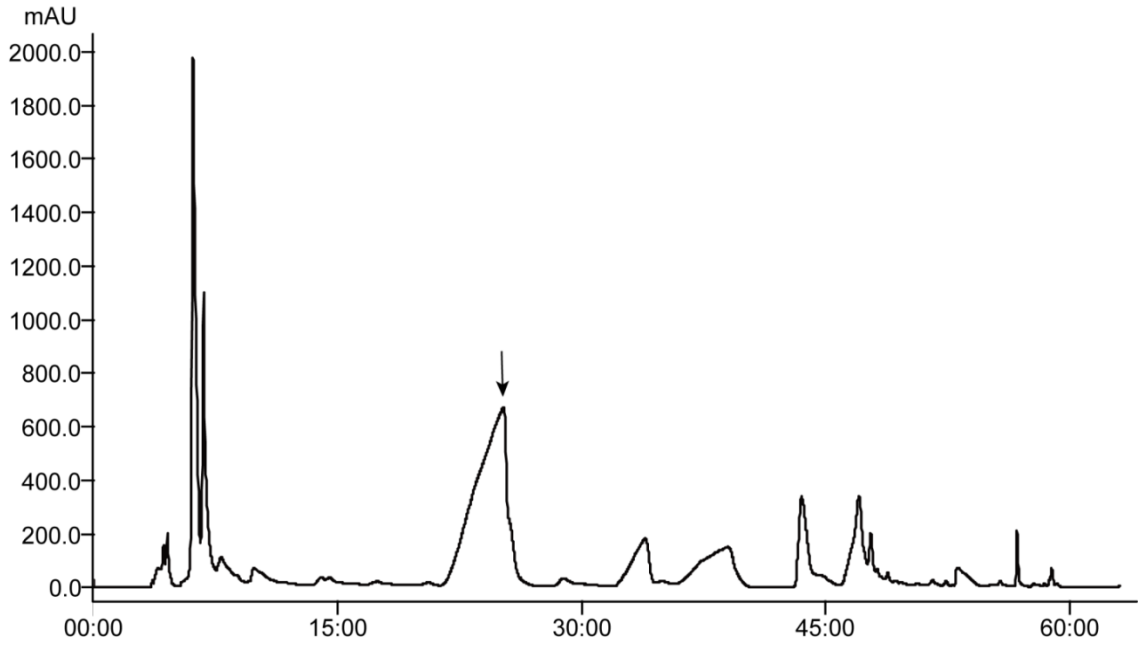


**Figure 5A**: Preparative HPLC chromatogram for **SylA** purification. Black arrow indicates the peak of **SylA**.[24]

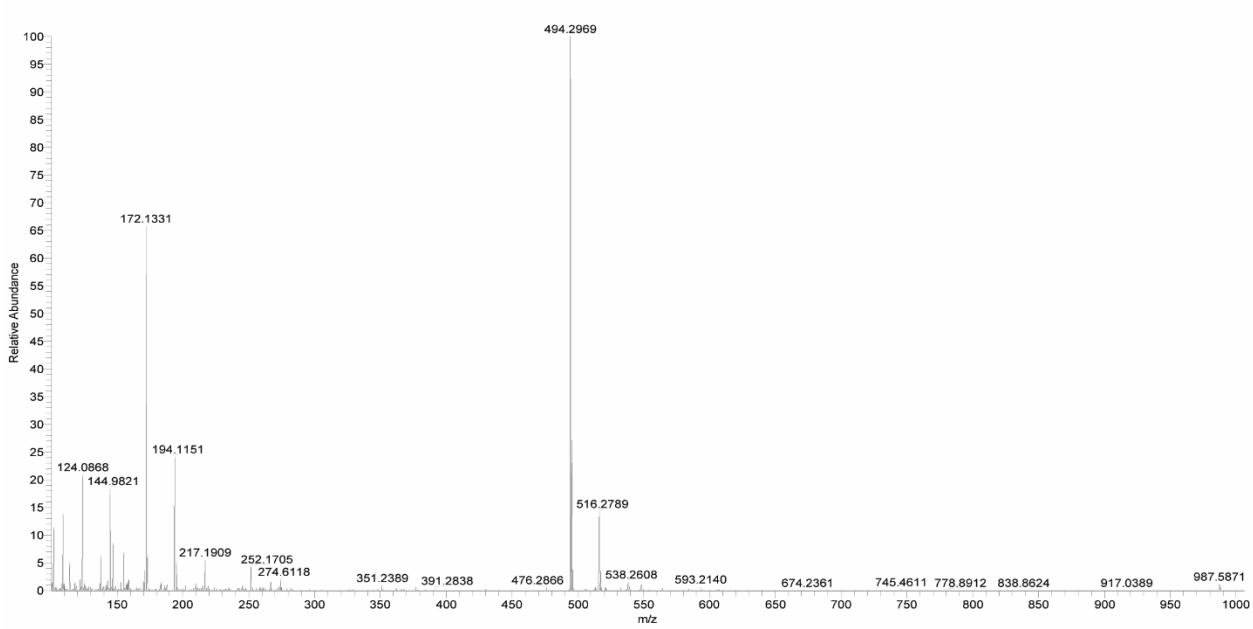


**Figure 5B**: HR-MS chromatogram of Syringolin A, after final purification. m/z = 494.2969.

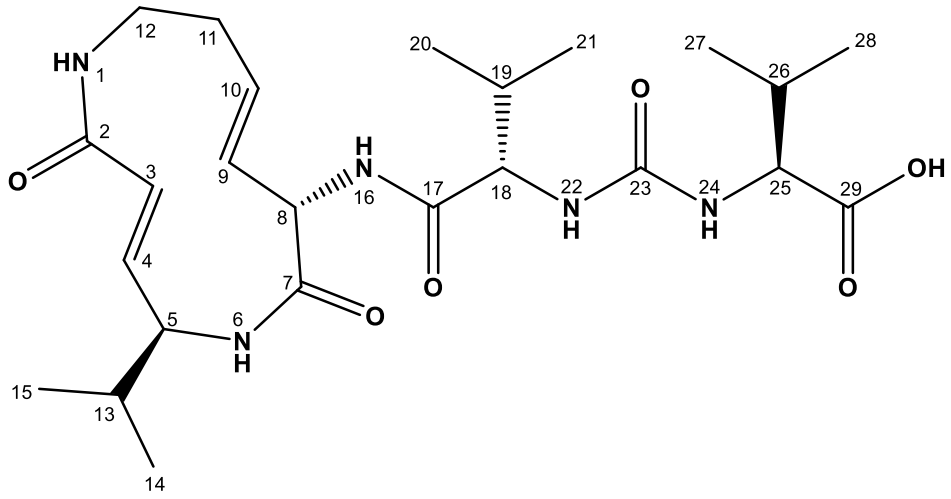


**Figure 6**: Structure elucidation of Syringolin A with NMR

The chemical shifts assignments for syringolin A were as follows (represented in **Figure 26**):

$^{1}$H NMR (600 MHz, d-DMSO): δ 8.03 (d, *J* = 7.30 Hz, 2 H, **6**, **16**), 7.47 (t, J = 7.2 Hz, 1 H, **1**), 6.68 (dd, J = 15.5, 5.5 Hz, 1 H, **4**), 6.30 (d, J = 8.6 Hz, 1 H, **22**), 6.25 (d, J = 9.0 Hz, 1 H, **24**), 6.09 (d, J = 15.2 Hz, 1 H, **3**), 5.59 (dt, J = 15.8, 7.6 Hz, 1 H, **10**), 5.41 (dd,

J = 15.6, 7.8 Hz, 1 H, **9**), 4.85 (m, 1 H, **8**), 4.02-4.12 (m, 2 H, **5**, **18**), 3.94 (dd, J = 8.8, 4.9 Hz, 1 H, **25**), 3.08- 3.25 (m, 2 H, overlapped with water, **12**), 2.23-2.32 (m, 1 H, **11**), 1.86-2.02 (m, 3 H, **11**, **19**, **26**), 1.68-1.78 (m, 1 H, **13**), 0.94 (d, J = 6.7 Hz, 3 H, **15**), 0.90 (d, J = 6.7 Hz, 3 H, **14**), 0.82-0.87 (m, 9 H, **20**, **21**, **27**), 0.77 (d, J = 6.9 Hz, 3 H, **28**);

$^{13}$C NMR (600 MHz, d-DMSO): δ 173.75 (**29**), 171.31 (**17**), 168.7 (**7**), 165.9 (**2**), 157.6 (**23**), 142.75 (**4**), 132.79 (**10**), 126.35 (**9**), 121.1 (**3**), 57.65 (**25**), 57.4 (**18**), 55.44 (**5**), 53.56 (**8**), 42.46 (**12**), 35.01 (**11**), 31.5 (**13**), 31.47 (**26**), 31.11 (**19**), 20.52 (**20**), 19.81 (**14**), 19.31 (**15**), 19.22 (**27**), 17.7 (**28**), 17.63 (**21**).

## Syringolin A probe synthesis

The probe design was of critical importance to the inhibitor screening, as drastically different probe would cause issues in proteasome inhibition and efficacy of Syringolin A. The non-essential part of Syringolin A activity was the tail, as the core was responsible for the covalent inhibition of the proteasome's beta subunits. The carboxylic acid moiety was modified with a peptide bond with an amine of 1-amino-3-butyne, without a change in stereochemistry as seen in **Figure 7A**. The synthesized Syringolin A probe (SylP) was characterized with HR-MS and NMR as shown in **Figure 7B** and **27**.

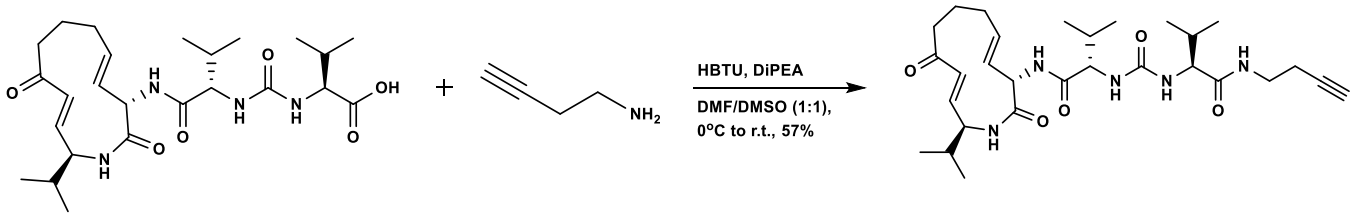


**Figure 7A**: Reaction of syringolin A (**SylA**) to form syringolin A probe (**SylP**).

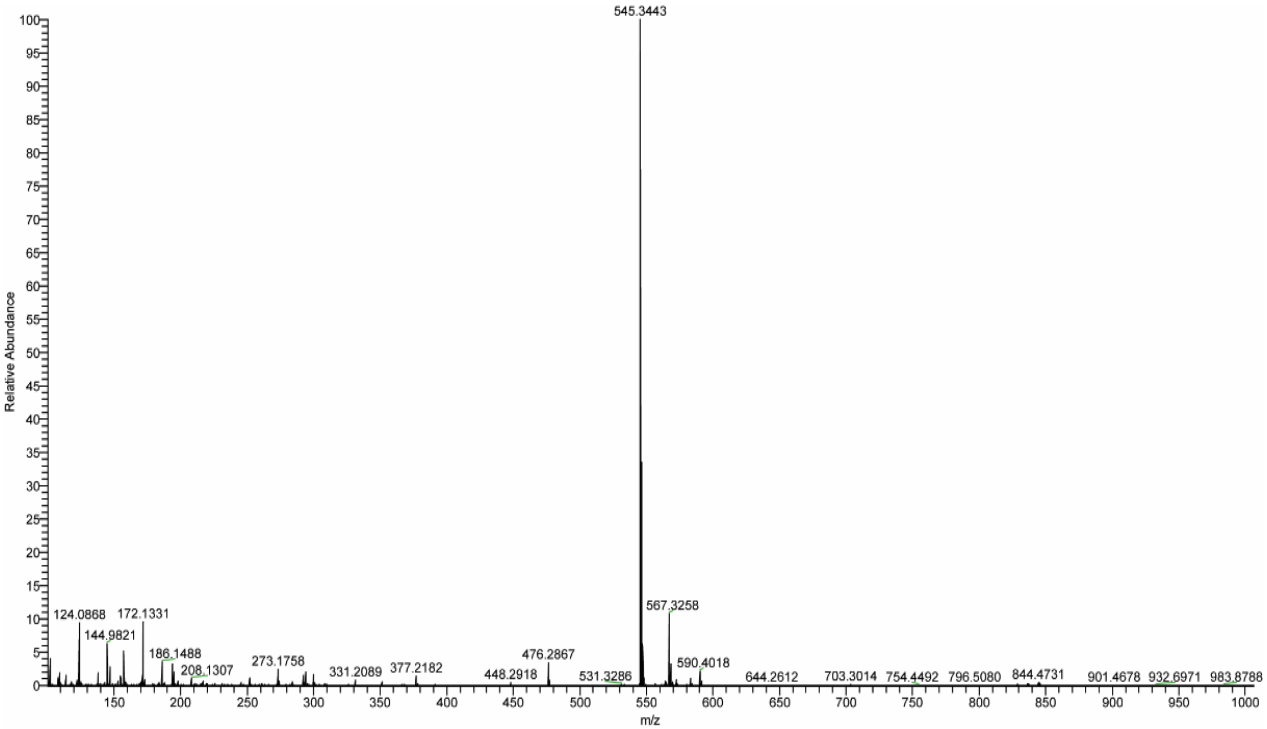


**Figure 7B**: HR-MS chromatogram of Syringolin A probe (**SylP**), HRMS m/z calculated for $C_{28}H_{45}N_6O_5$ $[M + H]^+$: 545.3451, found 545.3443, mass error = 1.4 ppm.

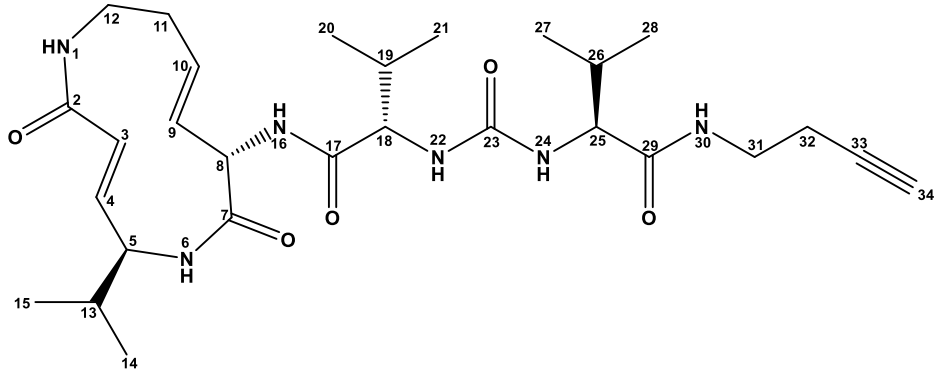

**Figure 8**: Structure elucidation of Syringolin A probe with NMR.

The Chemical shifts of syringolin A probe were as follows (represented in **Figure 27**):

$^{1}$H NMR (600 MHz, d-DMSO): δ 8.05 (m, 2 H, **6**, **30**), 7.93 (d, *J* = 6.6 Hz, 1 H, **16**), 7.45 (t, *J* = 6.64 Hz, 1 H, **1**), 6.69 (dd, *J* = 15.11, 5.24 Hz, 1 H, **4**), 6.28 (t, *J* = 8.25 Hz, 2 H, **22**, **24**), 6.09 (d, *J* = 15.58 Hz, 1 H, **3**), 5.56 (m, 1 H, **10**), 5.41 (m, 1 H, **9**), 4.83 (m, 1 H, **8**), 4.06 (m, 1 H, **5**), 4.00 (m, 1 H, **18**), 3.92 (m, 1 H, **25**), 3.22 (m, 1 H, **31**), 3.16 (m, 2 H, **12**), 3.09 (m, 1 H, **31**), 2.78 (s, 1 H, **34**), 2.26 (m, 3 H, **11**, **32**), 1.95 (m, 1 H, **11**), 1.91 (m, 1 H, **19**), 1.85 (m, 1 H, **26**), 1.73 (m, 1 H, **13**), 0.94 (d, *J* = 6.46 Hz, 3 H, **15**), 0.90 (d, *J* = 6.47 Hz, 3 H, **14**), 0.83 (d, *J* = 6.68 Hz, 3 H, **21**), 0.81 (d, *J* = 6.67 Hz, 3 H, **20**), 0.79 (d, *J* = 7.02 Hz, 3 H, **27**), 0.76 (d, *J* = 6.86 Hz, 3 H, **28**);

$^{13}$C NMR (600 MHz, d-DMSO): δ 172.03 (**29**), 171.6 (**17**), 168.97 (**7**), 166.42 (**2**), 157.65 (**23**), 143.47 (**4**), 133.15 (**10**), 126.0 (**9**), 121.21 (**3**), 82.10 (**33**), 72.10 (**34**), 58.00 (**25**), 57.69 (**18**), 55.59 (**5**), 53.66 (**8**), 42.61 (**12**), 37.74 (**31**), 35.07 (**11**), 31.57 (**13**), 31.26 (**26**), 30.93 (**19**), 19.87 (**14**), 19.43 (**15**), 19.35 (**20**), 19.29 (**21**), 18.73 (**32**), 17.87 (**27**), 17.68 (**28**).

## Limit of detection assay

To test the minimum required concentration of the inhibitor in the extracts, a limit of detection assay was performed with purified syringolin A. A serial dilution series of SylA was used (from 10 µM to 0.01 µM final conc.in assay) to competitively label mouse constitutive proteasome with SylP. The limit of detection was found to be between 5 and 1 µM, as seen in **Figure 9**. Due to the concentration of metabolites during extraction and evaporation of solvent, it would be suitable to detect using the competitive labelling strategy.

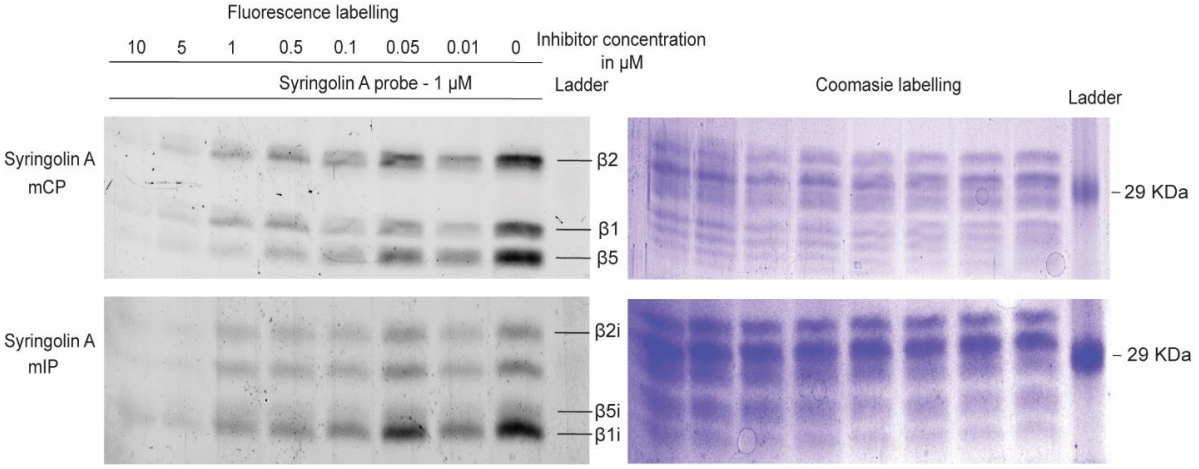


**Figure 9**: The detection limit of syringolin A, when competitively labeled with syringolin a probe. [24]

## Competitive labelling assay

The method used in this thesis is based on an activity-based protein profiling, aimed to elucidate new inhibitors of a/the proteasome. To achieve this, I incubated the proteasome with metabolic extracts from biological sources containing potential inhibitors, and after the initial binding, I added the competitive SylP probe to label the active sites of the proteasome. After the incubation period, I followed with the downstream steps of the click chemistry to tag the probe with a fluorescent dye - rhodamine azide (5-TAMRA) to visualize and analyze the sample on an SDS-PAGE gel via fluorescence scanning, as shown in **Figure 10**.

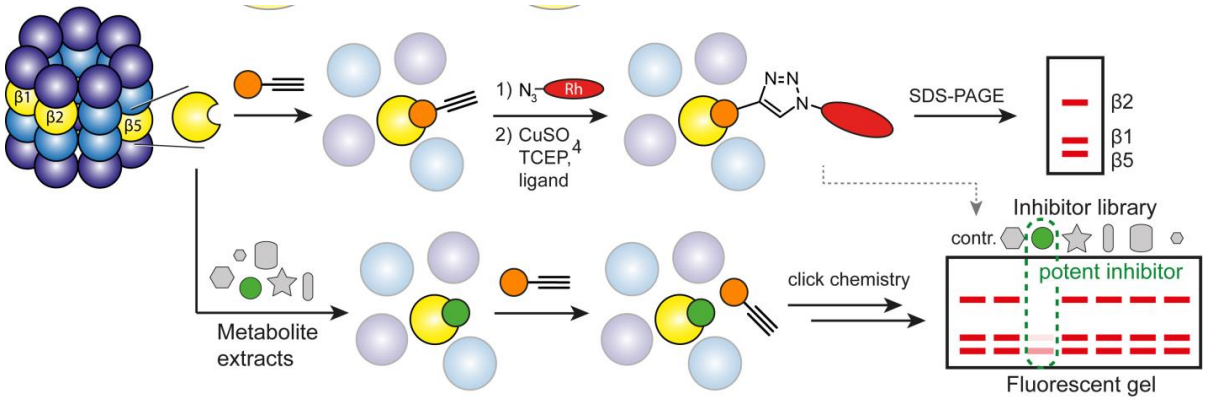


**Figure 10**: Competitive profiling strategy of natural product extracts for proteasome inhibitors. [24]

## Extraction and purification of syrbactins

The absence of protein bands in the fluorescence scans of the SDS-PAGE gels indicates the presence of an inhibitor in metabolic extracts. The extract can then be subjected to further purification methods, such as absorption with e.g. beads XAD -16N and preparative reverse phase HPLC. Each fraction of the chromatogram peaks was subjected to competitive labelling with SylP, and mouse constitutive proteasome. Inactive fractions were discarded and only the active fractions were advanced into the next round of purification. Repeating the procedure with purification based on the activity of the inhibitor makes the extraction activity guided and empirical as shown in **Figure 11** and **13**. Peaks I, J, K and L were active and subject to further purification.

Second round of purification involved a semi-preparative HPLC with better resolution and separation of peaks in the chromatogram. The individual peaks were collected separately and subjected to competitive labelling once more as shown in **Figure 14**. If the active fractions were deemed pure enough based on the peak characteristics, the samples were further subjected to NMR and HR-MS analyses. Peaks b, d and e were analyzed further with NMR and HR-MS.

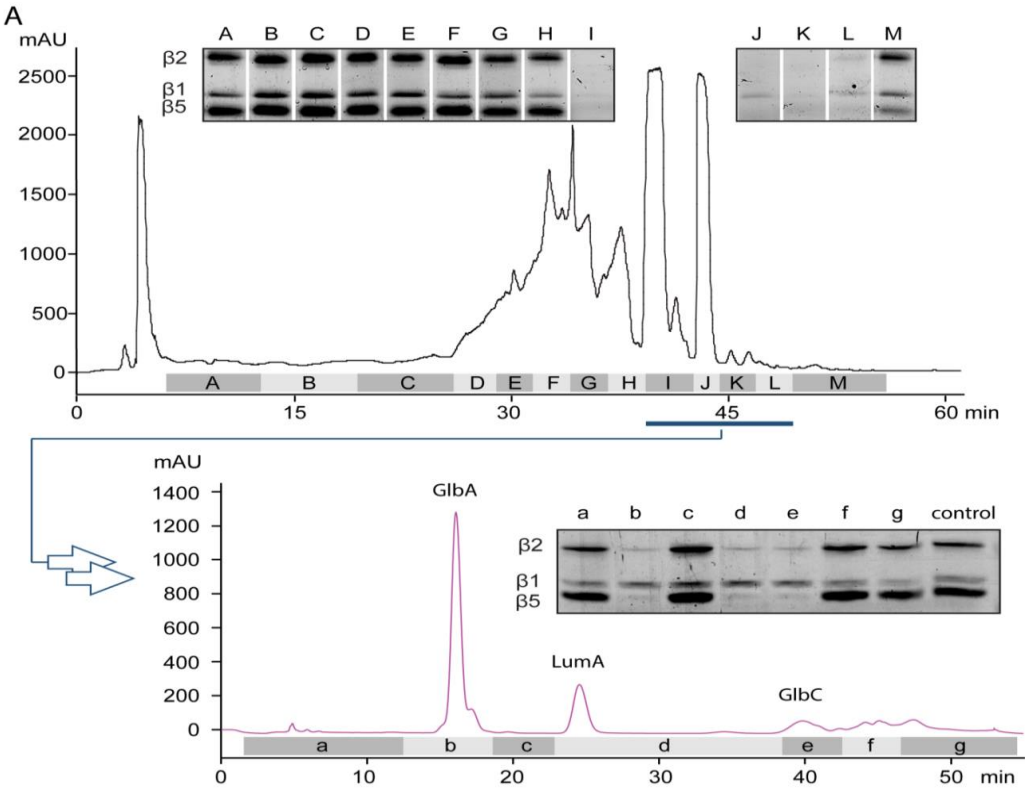


**Figure 11**: Fractionation of the crude metabolite extracts by preparative HPLC and

Competitive labeling was performed with a mouse CP against SylP. Representative fluorescent gel results of the competitive labeling of fractions A−M are displayed. Active fractions (G-L) were further purified by several rounds of semi-preparative HPLC runs and activity was assayed in SylP probe competition experiments with mouse CP. Fractions b, d, and e were purified to homogeneity. [24]

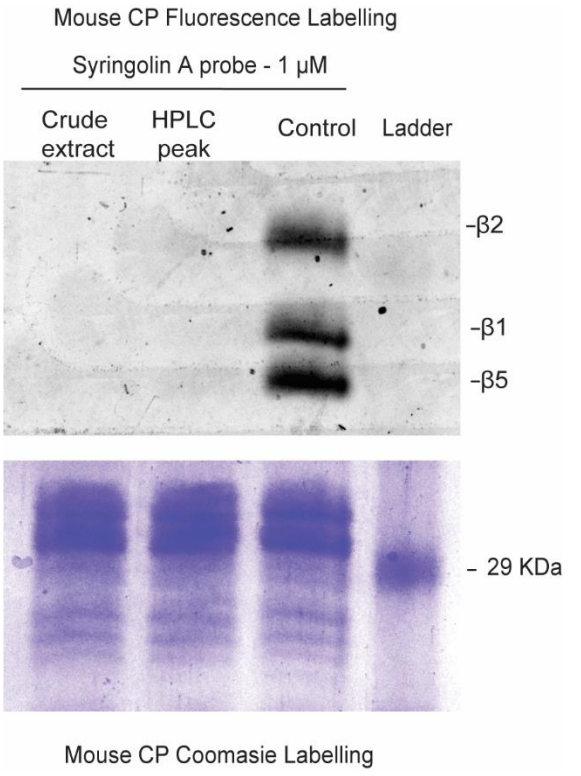


**Figure 12**: Representative competitive labelling of mCP with SylP, showing unknown active fraction crude extract and a representative HPLC peak. [24]

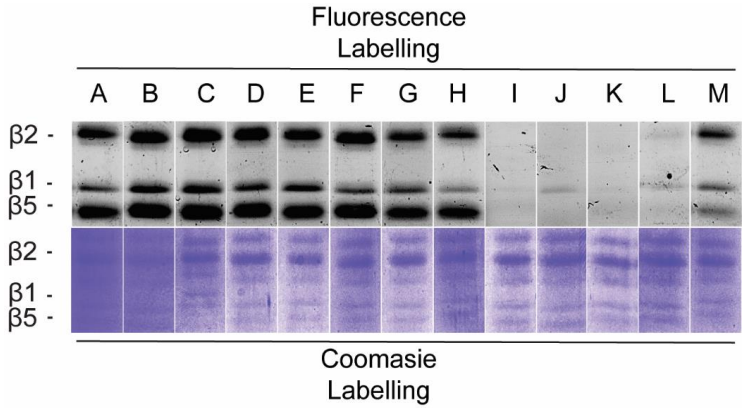


**Figure 13**: Competitive labelling of preparative HPLC peaks of purified crude extract. I, J, K, L showing inhibition of the proteasome due to lack to protein bands [24]

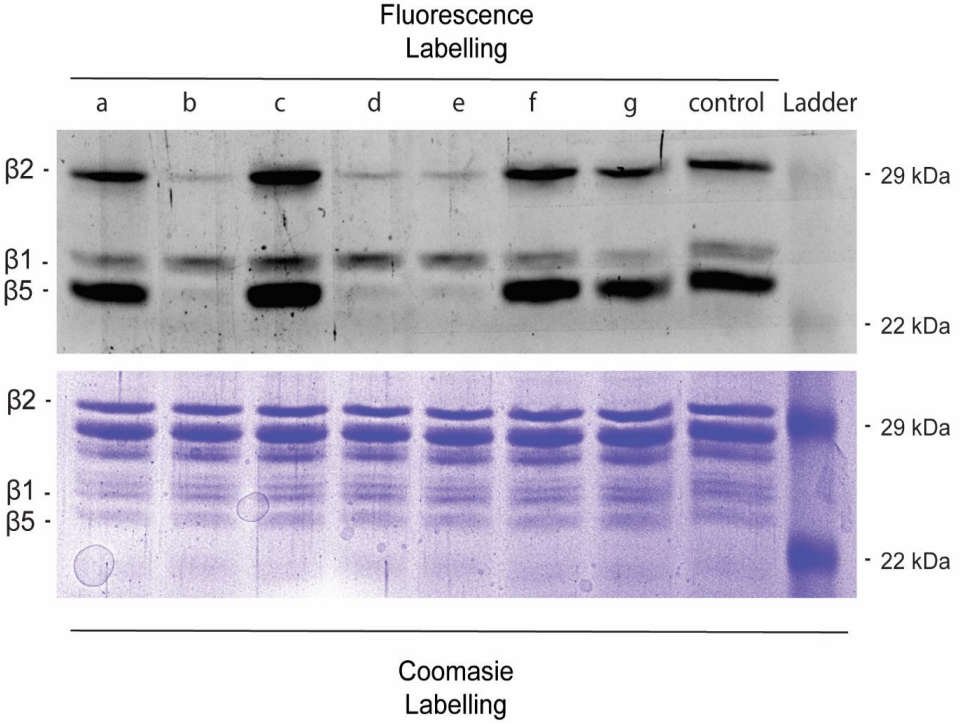


**Figure 14**: Competitive labelling of semi-preparative HPLC peaks of a previously active fraction. [24]

## Structure elucidation of isolated syrbactins

Chemical shifts were assigned to structure and identified using 1D and 2D NMR techniques, for each inhibitor as show in **Figure** 15, 16 and 17.

## Glidobactin A

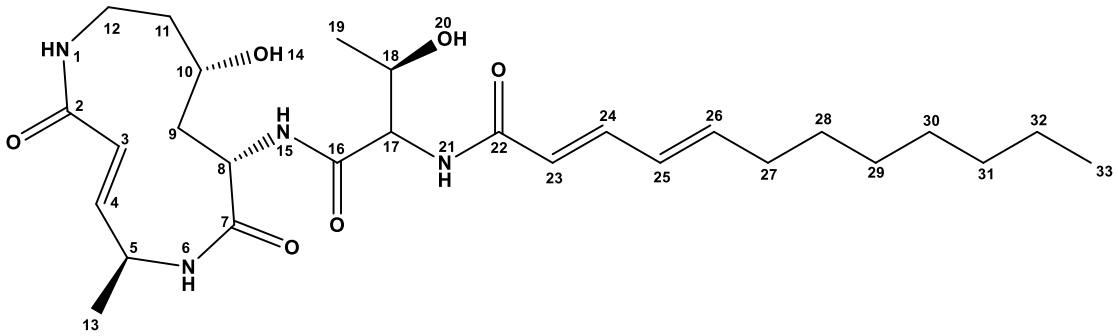


**Figure 15**: Structure elucidation of GlbA, with assigned chemical shifts in NMR (spectrum shown in **Figure 28**).

$^{1}$H NMR (600 MHz, DMSO-$d_6$): δ 8.63 (m, 1 H, **6**), 7.88 (d, *J* = 8.5 Hz, 1 H, **21**), 7.72 (d, *J* = 8.04 Hz, 1 H, **15**), 7.4 (t, *J* = 8.51 Hz, 1 H, **1**), 7.00 (dd, *J* = 10.93, 15.53 Hz, 1 H, **24**), 6.4 (d, *J* = 11.5 Hz, 1 H, **4**), 6.22 - 6.06 (m, 4 H, **3**, **23**, **25**, **26**), 4.82 (m, 1 H, **20**), 4.64 (m, 1 H, **14**), 4.39 (m, 1 H, **5**), 4.34 (m, 1 H, **8**), 4.29 (m, *J* = 11.5, 9.01 Hz, 1 H, **17**), 3.96 (m, 1 H, **18**), 3.57 (m, 1 H, **10**), 3.03 (m, 1 H, **12**), 2.98 (m, 1 H, **12**), 2.14 (q, *J* = 7.1 Hz, 2 H, **27**), 1.85 (m, 1 H, **9**), 1.58 (m, 1 H, **9**),1.45 (m, 1 H, **11**), 1.38 (m, 3 H, **11**, **28**), 1.30 – 1.23 (m, 8 H, **29**, **30**, **31**, **32**), 1.22 (m, 3 H, **13**), 0.99 (d, *J* = 6.3 Hz, 3 H, **19**), 0.86 (d, *J* = 6.64 Hz, 3 H, **33**)

$^{13}$C NMR (600 MHz, DMSO-$d_6$): δ 171.1* (**7**), 169.3* (**16**), 167.5* (**2**), 165.3* (**22**), 143.1 (**4**), 142.1 (**26**), 139.7 (**24**), 128.6 (**25**), 123.5 (**3**), 123.1 (**23**), 66.9 (**10**), 66.7 (**18**), 58.08 (**17**), 51.2 (**8**), 44.7 (**5**), 42.4 (**9**), 40.0 (**12**), 39.5* (**11**), 32.2 (**27**), 31.2 (**28**), 28.51 (**29**), 28.45 (**30**), 28.3 (**31**), 22.0 (**32**) 19.9 (**19**), 18.5 (**13**), 13.9 (**33**).

*carbon chemical shifts reported from HMBC data

HRMS m/z calculated for $C_{27}H_{45}N_4O_6$ $[M+H]^+$: 521.3339, found 521.3330, mass error = 1.7 ppm.

## Luminmycin A

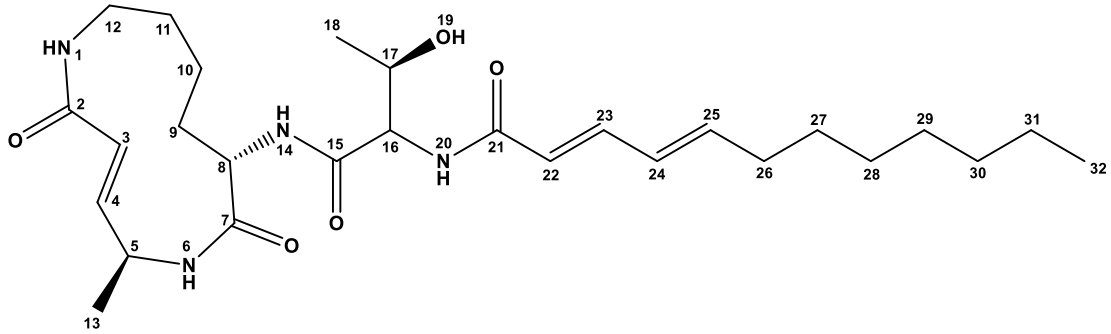

**Figure 16**: Structure elucidation of LumA with assigned chemical shifts in NMR (spectrum shown in **Figure 29**).

$^{1}$H NMR (600 MHz, DMSO-$d_6$): δ 8.45 (d, *J* = 8.02 Hz 1 H, **7**), 8.02 (dd, *J* = 8.5, 5.05 Hz 1 H, **20**), 7.63 (d, *J* = 7.1 Hz, 1 H, **14**), 7.35 (t, *J* = 6.99 Hz, 1 H, **1**), 6.99 (dd, *J* = 10.9, 15.5 Hz, 1 H, **23**), 6.78 (dd, *J* = 4.9, 15.3 Hz, 1 H, **4**), 6.25 - 6.06 (m, 4 H, **3**, **22**, **24**, **25**), 4.94 (m, 1 H, **19**), 4.52 (m, 1 H, **8**), 4.40 (m, 1 H, **5**), 4.32 (m, 1 H, **16**), 3.98 (m, 1 H, **17**), 3.3 (m, 1 H, **12**), 2.94 (m, 1 H, **12**), 2.12 (m, 2 H, **26**), 2.06 (m, 1 H, **9**), 1.68 (m, 1 H, **9**), 1.44 (m, 2 H, **11**), 1.31 (m, 2 H, **10**), 1.38(m, 2 H, **27**), 1.28 (m, 2 H, **31**),1.25 (m, 6 H, **28**, **29**, **30**), 1.20 (d, *J* = 6.9 Hz, 3 H, **13**), 1.02 (d, *J* = 6.6 Hz, 3 H, **18**), 0.86 (t, *J* = 8.6 Hz, 3 H, **32**).

$^{13}$C NMR (600 MHz, DMSO-d6): δ 171.60 (**7**), 169.52 (**15**), 167.8 (**2**), 165.60 (**21**), 147.1* (**4**), 142.36 (**25**), 139.97 (**23**), 128.65 (**24**), 123.1 (**22**), 118.2 (**3**), 66.80 (**17**), 58.23 (**16**), 51.3 (**8**), 44.87 (**5**), 37.40 (**12**), 32.30 (**26**), 31.34 (**11**), 29.01 (**9**), 28.65, 28.61, 28.60, 28.45 (**27**, **28**, **29**, **30**), 22.19 (**31**), 20.03 (**18**), 18.64 (**13**), 17.30 (**10**), 14.08 (**32**). *carbon chemical shifts reported from HMBC data

HRMS m/z calculated for $C_{27}H_{45}N_4O_5$ [M+H]+ 505.3389, found 505.3378, mass error = 2.1 ppm.

## Glidobactin C

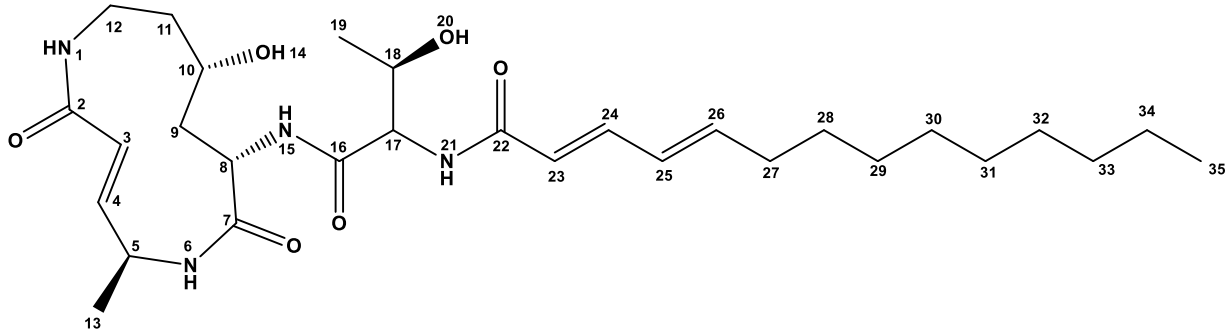


**Figure 17**: Structure elucidation of GlbC with assigned chemical shifts in NMR (spectrum shown in **Figure 30**).

$^{1}$H NMR (600 MHz, DMSO-$d_6$): δ 8.66 (m, 1 H, **6**), 7.89 (d, *J* = 8.7 Hz, 1 H, **21**), 7.70 (d, *J* = 7.9 Hz, 1 H, **15**), 7.40 (d, *J* = 8.6 Hz, 1 H, **1**), 6.99 (dd, *J* = 15.2, 10.3 Hz, 1 H, **24**), 6.39 (m, 1 H, **4**), 6.05 – 6.23 (m, 4 H, **3**, **23**, **25**, **26**), 4.84 (d, *J* = 5.26 Hz, 1 H, **20**), 4.65 (d, *J* = 4.9 Hz, 1 H, **14**), 4.36 (m, 2 H, **8**, **5**), 4.29 (q, *J* = 4.3 Hz, 1 H, **17**), 3.96 (m, 1 H, **18**), 3.57 (m, 1 H, **10**), 2.99 (m, 2 H, **12**), 2.13 (dd, *J* = 7.0, 14.5 Hz, 2 H, **27**), 1.85 (m, 1 H, **9**), 1.58 (m, 1 H, **9**), 1.44 (m, 1 H, **11**), 1.37 (m, 3 H, **11**, **28**), 1.25(m, 12 H, **29**, **30**, **31**, **32**, **33**, **34**), 1.20 (m, 3 H, **13**), 0.99(d, *J* = 6.26 Hz, 3 H, **19**), 0.85(t, *J* = 7.1 Hz, 3 H, **35**).

$^{13}$C NMR (600 MHz, DMSO-d6): δ 171.1* (**7**), 169.3* (**16**), 167.5* (**2**), 165.44* (**21**), 143.2 (**4**), 142.1 (**25**), 139.7 (**23**), 128.6 (**3**, overlapped), 128.5 (**24**, overlapped), 123.1 (**22**), 66.9 (**18**), 66.7 (**10**), 58.11 (**17**), 51.2 (**8**), 44.7 (**5**), 42.4 (**9**), 39.7* (**12**), 39.4* (**11**), 32.3 (**27**), 29.04 (**29**), 28.97 (**30**), 28.87 (**31**), 28.71 (**32**), 28.61 (**33**), 28.4 (**28**), 22.01 (**34**), 19.9 (**19**), 18.5 (**13**), 13.9 (**35**).

*carbon chemical shifts reported from HMBC data

HRMS (ESI) m/z calculated for C29H49N4O6 [M+H]+ 549.3652, found 549.3645, mass error = 1.2 ppm.

## Concentration gradient competitive labelling and Fluorogenic substrate hydrolysis assay.

Each of the inhibitors was subjected to dose response competitive labelling ranging from 10 µM to 0.01 µM final concentrations in assay, with an alternating dilution ratio of 1:2 and 1:5. The SylP was kept at constant concentration of 1 µM and labelling was carried out for both mouse CP and IP. Pure DMSO was used as a negative control.

For the mouse Constitutive proteasome, each of the inhibitors displayed intra- and inter-subunit specificity. GlbA and GlbC showed similar inhibition patterns owing to their similar core structural characteristics. LumA was different compared to GlbA and GlbC, as it was less potent against β2, as shown in **Figure 18A**.

In case of the mouse Immunoproteasome, GlbA showed better inhibition of β2i than GlbC and LumA. GlbA and GlbC were similar in specificity and potency for β1i and β5i. LumA was similar in all subunit specificity; however, was less potent overall when compared to GlbA and GlbC as show in **Figure 18B**.

Based on these results, it was clear that the inhibitors showed differential subunit preference and specificity. The pattern of inhibition was quite remarkable and warranted more detailed analysis.

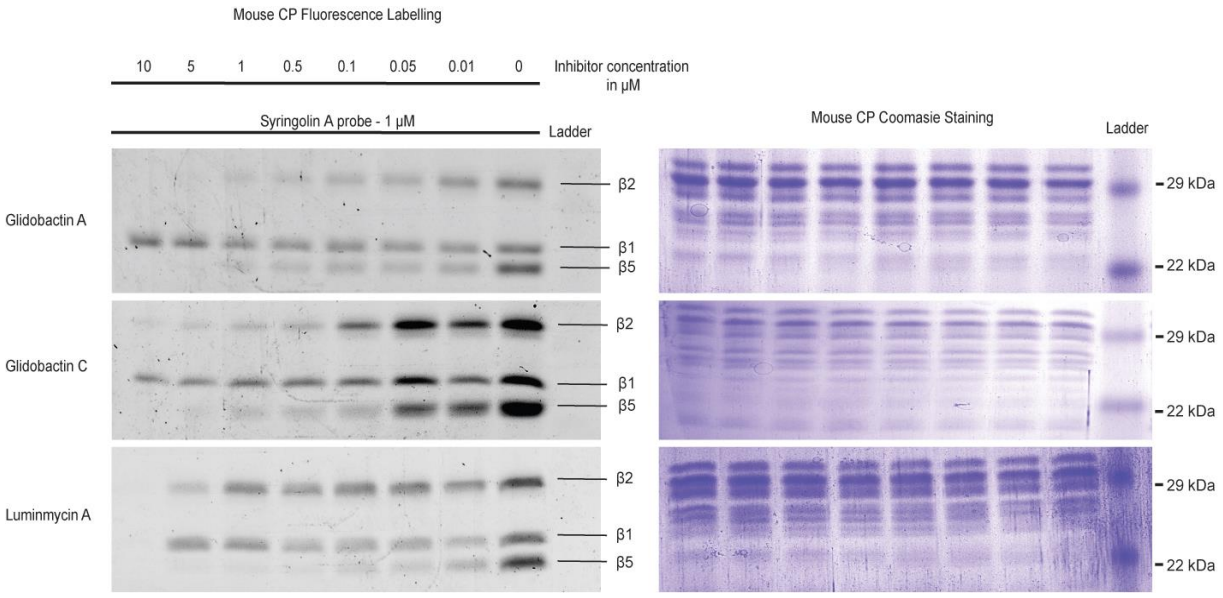


**Figure 18A**: Dose response inhibition of GlbA, GlbC and LumA, observed during competitive labelling assay with mCP. Both fluorescence scanning and Coomasie stained gel images are show. [24]

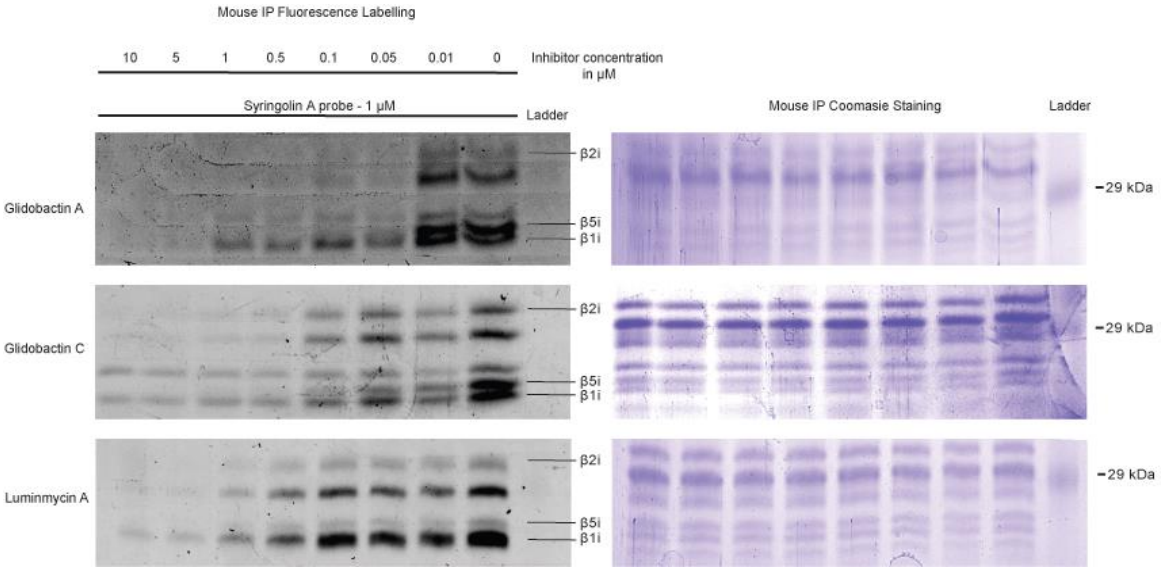


**Figure 18B**: Dose response inhibition of GlbA, GlbC and LumA, observed during competitive labelling assay with mIP. Both fluorescence scanning and Coomasie stained gel images are show. [24]

## Fluorogenic substrate hydrolysis assay

To further investigate the previous results of differential subunit specificity, subunit specific Fluorogenic substrates were cleaved using both the human and the mouse constitutive proteasomes and immunoproteasome.[27] GlbA and GlbC documented high specificity for mouse β2i with $IC_{50}$ of concentration of 1.4 nM and 15 nM respectively, while mouse β2 remaining unaffected as shown in **Table 1**.

Both GlbA and GlbC inhibited β5 of both the human and mouse constitutive proteasome with $IC_{50}$ of concentration of 3.6 nM and 0.6 nM for GlbA, for GlbC 2.9 nM and 2.7 respectively. As expected from the competitive labelling experiments, LumA was much less potent than both GlbA and GlbC, although it had similar inhibition pattern across all β5/ β5i and β2/β2i subunits.

The results confirm the previous hypothesis that GlbA and GlbC show the potency and substrate specificity towards β2 and β5. With these interesting results, I proceeded with cell based assays. Work for Fluorogenic substrate hydrolysis assay was performed in collaboration with AG Groettrup, University of Konstanz.

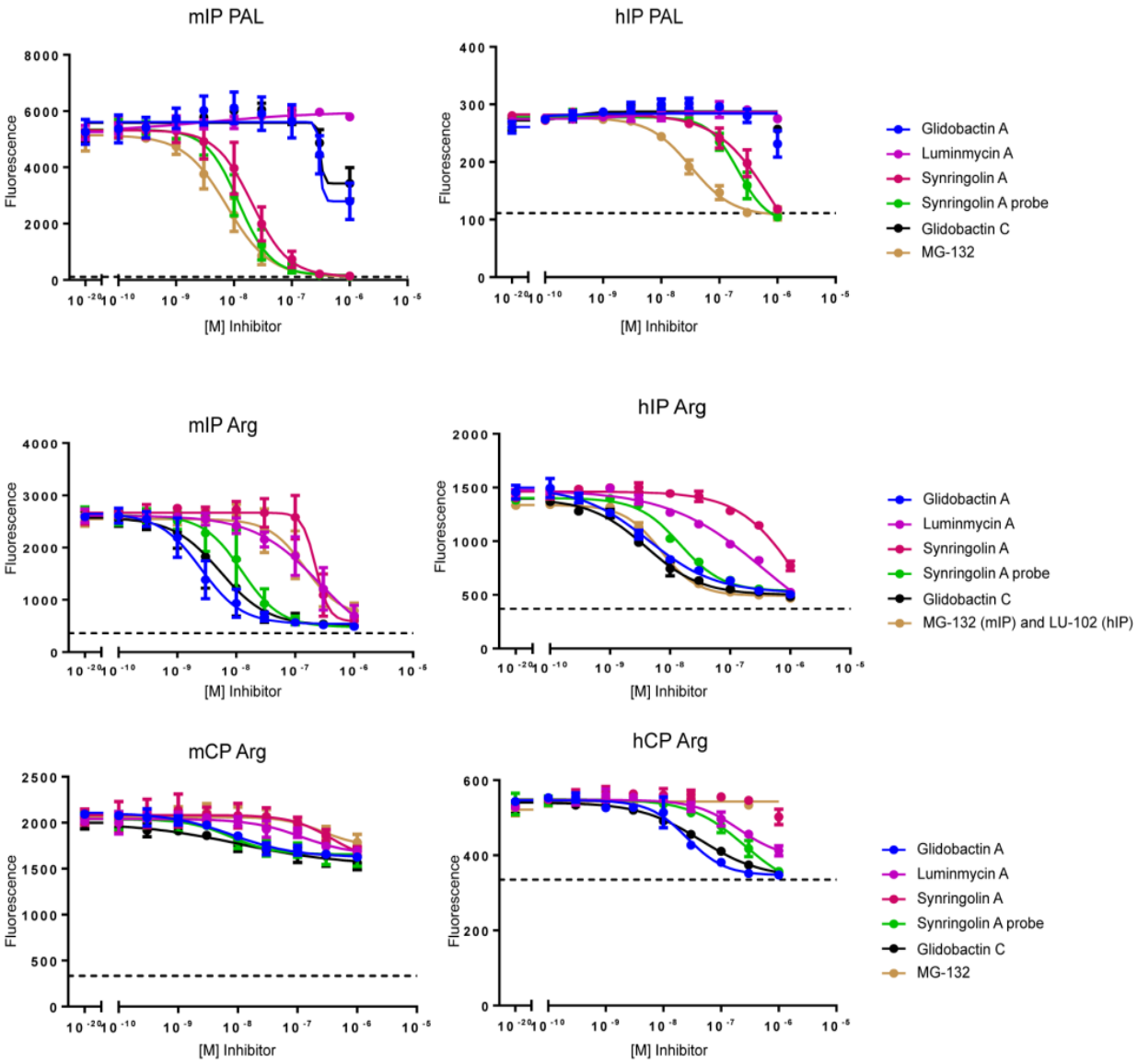


**Figure 19**: Continued on next page.

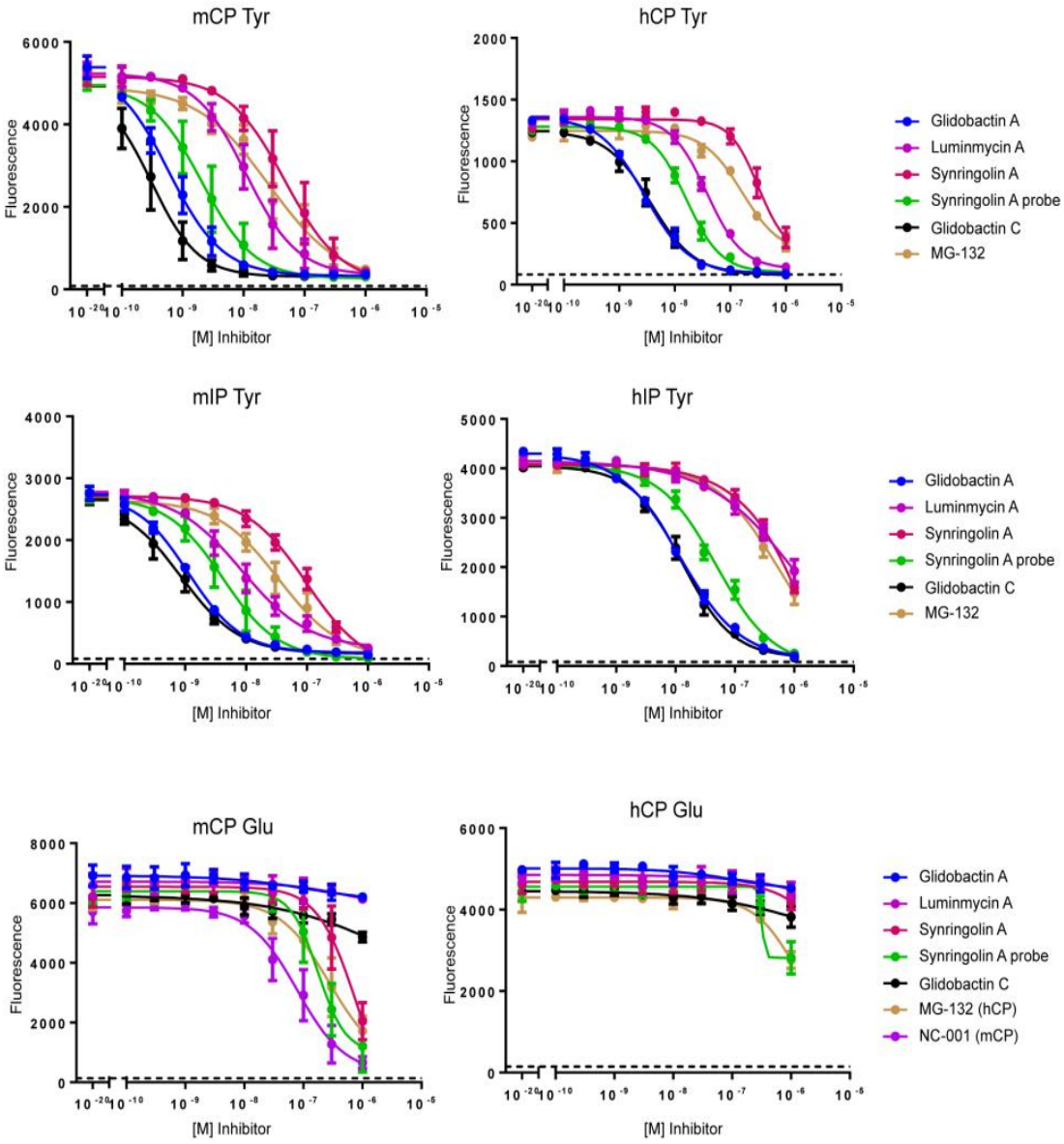


**Figure 19**: Inhibition assay with Fluorescence substrate for Glidobactin A (Blue), Luminmycin A (Pink), Syringolin A (Red), Syringolin A probe (Green), Glidobactin C (Black) and with MG-132 or LU-102 (Gold) or NC-001 (Purple) as positive control A. [24]

| Activity / Species | | Proteasome | SylA | SylP | LumA | GlbA | GlbC |
|---|---|---|---|---|---|---|---|
| Chymotrypsin -like activity (β5/β5i)* | human | CP | $1.8 \pm 1.1\ 10^{-7}$ | $1.0 \pm 0.8\ 10^{-8}$ | $3.9 \pm 0.2\ 10^{-8}$ | $3.6 \pm 1.1\ 10^{-9}$ | $2.9 \pm 2.2\ 10^{-9}$ |
| | | IP | $2.4 \pm 1.9\ 10^{-6}$ | $3.6 \pm 1.8\ 10^{-8}$ | $1.6 \pm 0.6\ 10^{-6}$ | $2.5 \pm 1.9\ 10^{-8}$ | $7.1 \pm 5.3\ 10^{-9}$ |
| | mouse | CP | $5.9 \pm 1.6\ 10^{-8}$ | $2.1 \pm 0.0\ 10^{-9}$ | $3.2 \pm 2.9\ 10^{-8}$ | $6.5 \pm 0.8\ 10^{-10}$ | $2.7 \pm 3.4\ 10^{-9}$ |
| | | IP | $1.8 \pm 2.0\ 10^{-7}$ | $3.2 \pm 1.9\ 10^{-9}$ | $8.9 \pm 0.6\ 10^{-9}$ | $1.1 \pm 0.1\ 10^{-9}$ | $1.3 \pm 0.7\ 10^{-9}$ |
| Trypsin-like activity (VGR) (β2/β2i)* | human | CP | n.i. | $1.4 \pm 1.8\ 10^{-7}$ | $2.6 \pm 0.8\ 10^{-7}$ | $1.5 \pm 1.5\ 10^{-8}$ | $2.4 \pm 2.8\ 10^{-8}$ |
| | | IP | $6.7 \pm 7.5\ 10^{-7}$ | $1.6 \pm 0.2\ 10^{-8}$ | $1.7 \pm 1.6\ 10^{-7}$ | $4.2 \pm 0.8\ 10^{-8}$ | $2.5 \pm 2.0\ 10^{-9}$ |
| | mouse | CP | n.i. | n.i. | n.i. | n.i. | n.i. |
| | | IP | n.i | $1.1 \pm 1.4\ 10^{-7}$ | n.i. | $1.4 \pm 1.6\ 10^{-9}$ | $1.5 \pm 1.3\ 10^{-8}$ |
| Caspase-like activity (β1)* | human | CP | n.i. | n.i. | n.i. | n.i. | n.i. |
| | mouse | CP | $5.0 \pm 7.0\ 10^{-5}$ | $2.1 \pm 0.5\ 10^{-7}$ | n.i. | n.i. | n.i. |
| LMP2 activity (β1i)* | human | IP | $7.6 \pm 0.0\ 10^{-7}$ | $1.7 \pm 0.6\ 10^{-7}$ | n.i. | n.i. | n.i. |
| | mouse | IP | $2.8 \pm 1.0\ 10^{-8}$ | $2.2 \pm 1.5\ 10^{-8}$ | n.i. | $2.5 \pm 0.8\ 10^{-7}$ | n.i. |

**Table 1**: $IC_{50}$ concentration, data derived from **Figure 20**, $IC_{50}$ values of inhibitors in mol/L.

# Results: Cell based assays – *in vivo* exploration of differential activity of inhibitors

## Cell permeability assay

To proceed with the *in-vivo* experiments, the ability of inhibitors to permeate the cell membrane was an important question to be answered. LCL721.145 cells were used in this assay and were treated with a specified concentration of the GlbA, GlbC (B), LumA, SylA, and SylP (A). MG132 was used as a positive control for the assay. The assay count was determined by hydrolysis of a well-known cell permeable substrate, MeOSuc-GLF-AMC. The assay was performed twice in triplicates (n=6). Based on the results in **Figure 20**, only GlbC was found to be cell permeable. Work for cell based experiments was performed in collaboration with AG Groettrup, University of Konstanz.

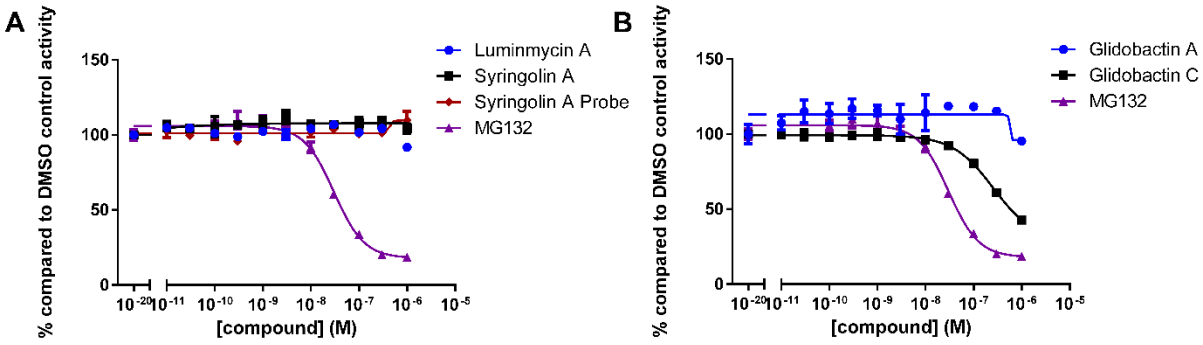


**Figure 20**: Cell permeability assay with Luminmycin A, Syringolin A, Syringolin A probe (A) and Glidobactin A and Glidobactin C (B). The mean ± SD % activity compared to DMSO control is displayed.[24]

## Ubiquitin-protein conjugate accumulation assay

To further test the activity in live cells, mouse fibrosarcoma MC57 cells were treated with GlbC for 6 h, along with MG132 as positive control and DMSO as negative control. The resulting accumulated ubiquitin conjugates in the cell showed GlbC concentration dependence and better conjugate formation than positive control of MG-132, as shown in **Figure 21**. Work for cell based experiments was performed in collaboration with AG Groettrup, University of Konstanz.

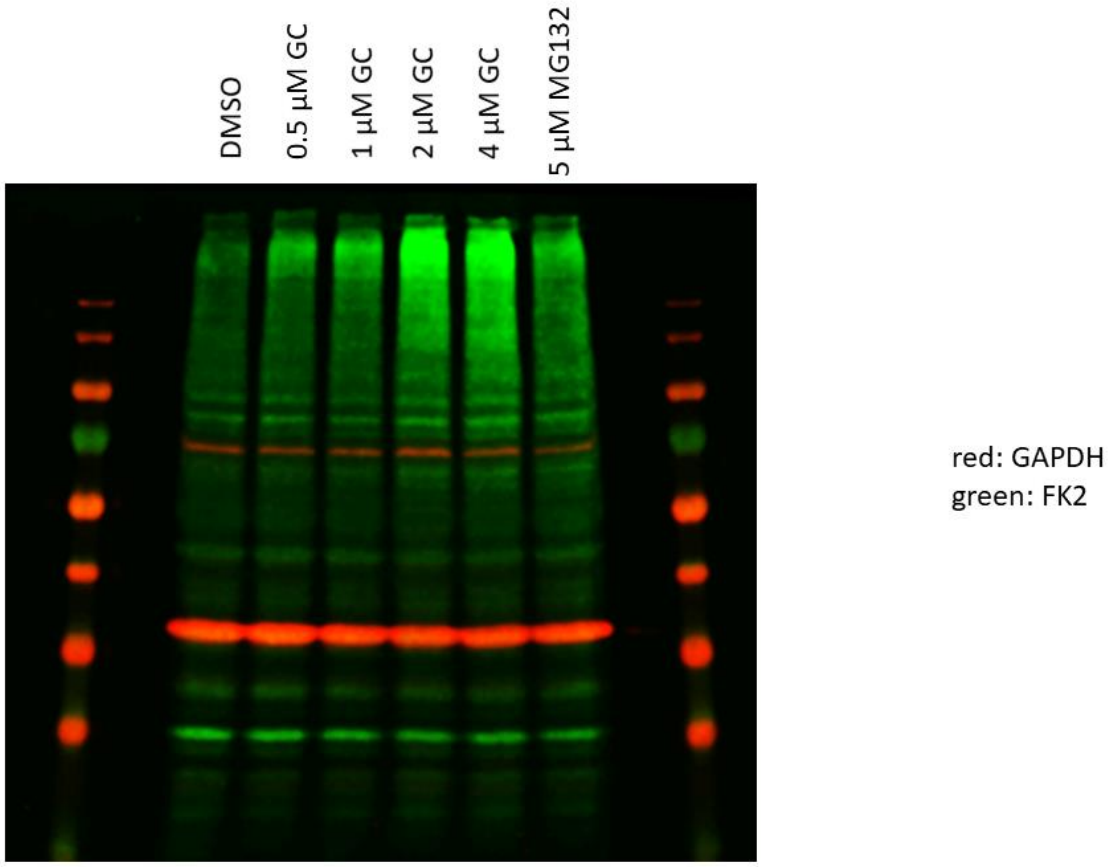


**Figure 21**: The ubiquitin−protein conjugates accumulate upon GlbC treatment, as visualized by the Western blot analysis with mAb FK2. Loading control: GADPH; positive control: proteasome inhibitor MG132.

## ELISA analysis of IL-6 in culture supernatant

Based on the accumulation of ubiquitin conjugates, it was deemed interesting to studying the effect on inflammatory responses in the cell. The cells were treated with indicated concentration of GlbC and ONX 0914 (positive control, specific inhibitor of LMP 2/7), subsequently, the cells were exposed to 1 µg/ml LPS (from *Escherichia coli* 0111:B4). The Interleukin 6 in the media supernatant was analyzed with ELISA. The assay was performed twice in triplicates. **Figure 22** shows the results of the assay performed. Work for cell based experiments was performed in collaboration with AG Groettrup, University of Konstanz.

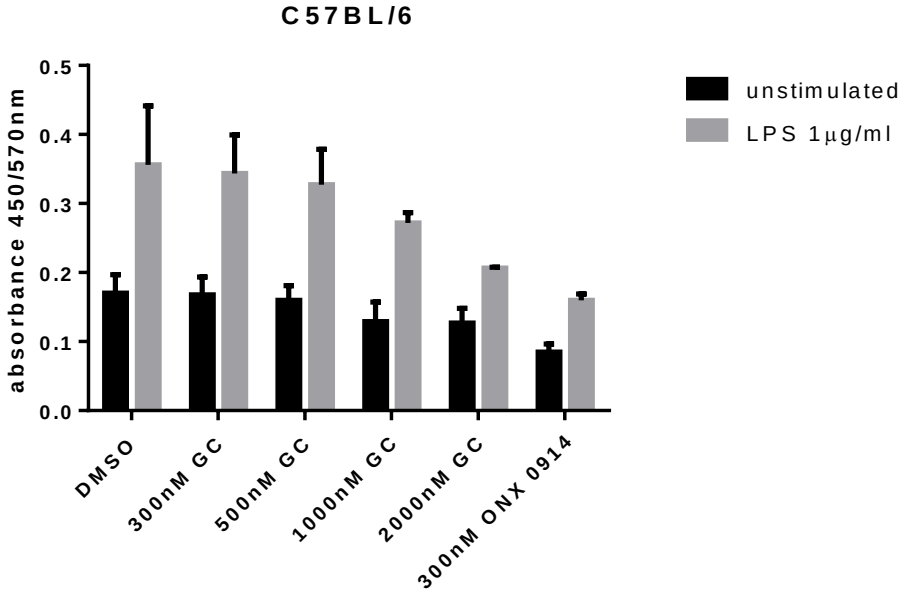


**Figure 22**: ELISA result from presence of IL-6 in the culture supernatant of C57BL/6 mouse splenocytes treated with GlbC. Positive control used: LMP 2/7 specific inhibitor ONX 0914.

## Cell viability assay of breast cancer cell lines

To determine the potential of GlbC in anti-cancer therapy, and investigate its effect on solid tumors, three breast cancer cell lines, BT-549, MDA-MB-231, and MDA-MB-36, were chosen, as these cell lines require β2/β5 coinhibition for cell growth suppression. The dotted line represents the initial seeding of the cells ($5*10^4$ for BT-549, $10*10^4$ for MDA-MB-231, and MDA-MB-36). The 0.25 µM GlbC treatment showed inhibition of cell proliferation and higher concentration caused cell death as indicated in **Figure 23**. Work for cell based experiments was performed in collaboration with AG Groettrup, University of Konstanz.

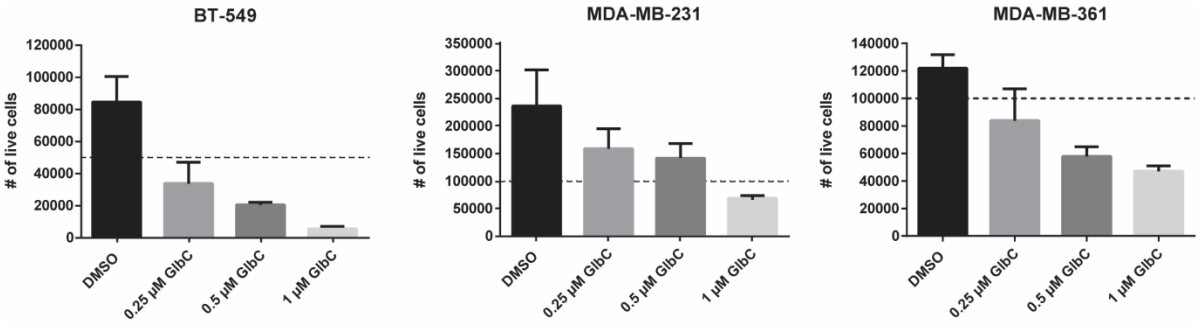


**Figure 23**: Cell counting assay, after 48 h for treatment of breast cancer cell line BT-549, MDA-MB-231, and MDA-MB-361 with GlbC.

## T-cell proliferation assay

To verify, if the GlbC affects the T-cells growth in the wild type cells, compared to immunoproteasome deficient T-cells, a cell division study of $CD4^+$ T-cells after T-cell receptor (TCR) stimulation was conducted. Splenocytes derived $CD4^+$ T-cells from C57BL/6 mice were used as wildtype cells and Splenocytes derived $CD4^+$ T-cells from MECL-$1^{-/-}$/LMP$7^{-/-}$ mice were used as immunoproteasome deficient cells. Bortezomib was used as a reference compound. Although there is a dose dependent inhibition of T-cells with GlbC treatment, there was no difference found in wildtype cells compared to immunoproteasome deficient cells. Compared to Bortezomib, GlbC shows much lower inhibition of the cell division as per data in **Figure 24**. Work for cell based experiments was performed in collaboration with AG Groettrup, University of Konstanz.

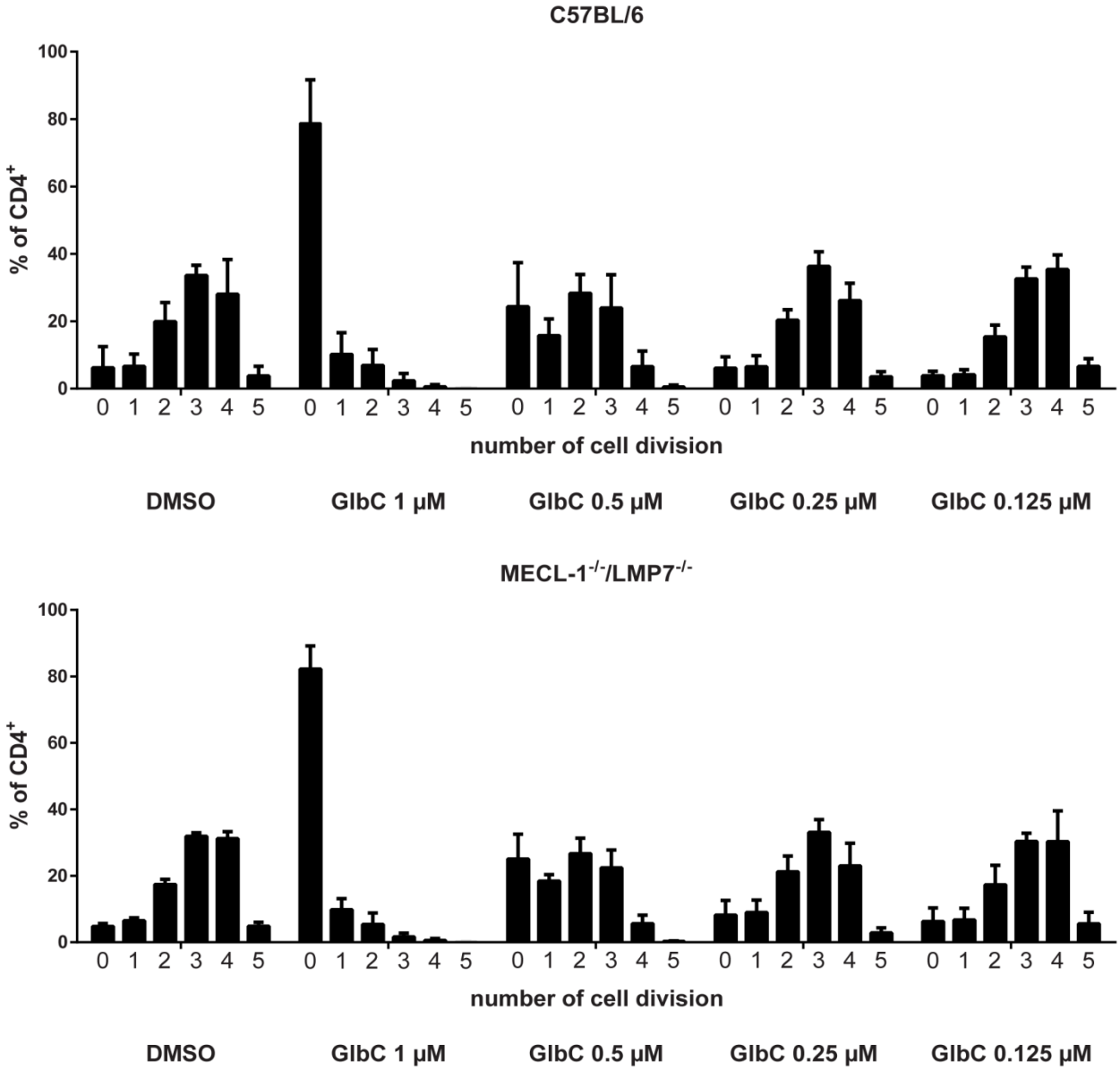

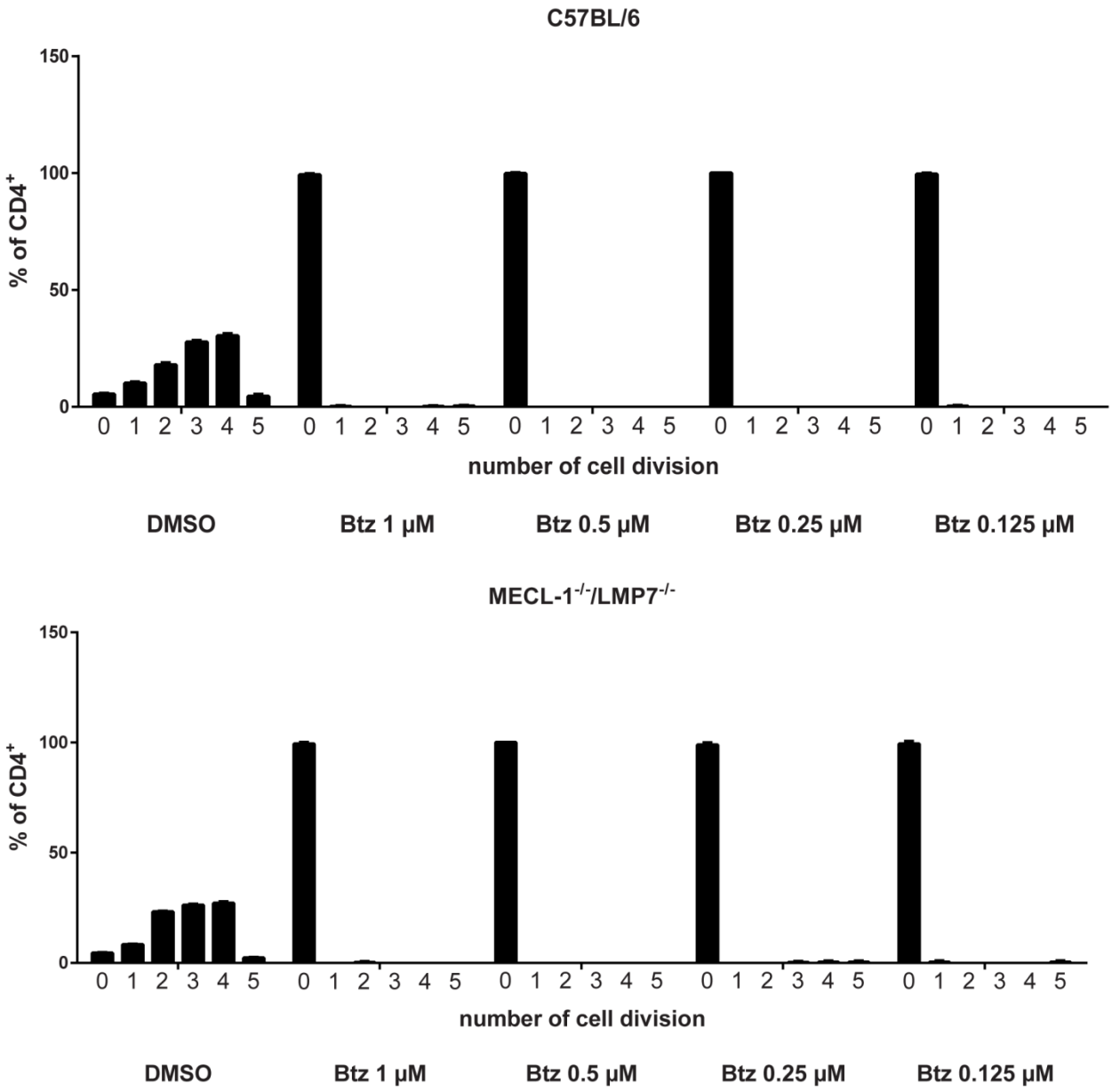


**Figure 24**: $CD4^+$ T-cells derived from C57BL/6 wildtype mice or MECL-$1^{-/-}$/LMP$7^{-/-}$ double deficient mice were treated with GlbC and Bortezomib at varying concentrations. The stimulation was carried out with plate-bound antibodies to CD3/CD28. After 65 h after stimulation the CFSE dilution of $CD4^+$ cells was analyzed via flow cytometry. X-axis represent cell division (0- 5), Y-axis represents % of $CD4^+$ cells with +/- S.D. experiments were carried out in triplicates.

# Conclusion

This thesis reports an unanticipated low nanomolar range of the β2/β5 co-inhibition in mouse immunoproteasome by Glidobactin C. Along with potent cell permeability; Glidobactin C makes a promising anti-cancer drug candidate. Not only Glidobactin C has a potential for a therapeutic use, but also its use as a proteomic tool for subunit specificity inhibition in the proteasome. Glidobactin C has a potential to be used as a base scaffold structure to develop similar molecules, which could have better cell permeability, subunit specificity and inhibition profile. Until now, Glidobactin C presents itself to be the only natural product inhibitor able to inhibit both β5/β5i and β2/β2i subunits of the human constitutive and the immunoproteasome respectively in low nanomolar range. It is known, that combining inhibition of β5/ β5i and β2/β2i subunits together, limits the growth and proliferation of breast, lung, kidney and ovarian cancer cells.[25] Since Glidobactin C fulfills this criterion, it would be interesting to test its efficacy against other solid cancer and tumor cell lines. Given the similar core structures of syrbactins, slight structural variations can have influence on the subunit and species selectiveness of these inhibitors.

The above results clearly show the potential of direct application of the competitive protein profiling via development of the active-site directed- natural products as chemical probes. With this strategy it is possible to identify, isolate and provide preliminary observations for subunit specificity for inhibitors of proteasome catalytic subunits. The SylP developed in this research displays similar activity to natural product inhibitor SylA, which is an advantage as the modification of the tail with an alkyne moiety does not limit its inhibition. Any bulky labelling molecules can later be tagged via click reactions after denaturing the proteasome.

Based on the results, it is shown that in syrbactins, structural geometry of the core governs subunit selectivity, while the tail region influences efficacy and cell permeability. These findings suggest that even within an organism, each of the inhibitors might have a specialized functional role based on its structure.

From the biological perspective, the differences in structures of syrbactins represents a unique adaptation for the producers of syrbactins to interact, infect their targets and survive in ecological niche as plant pathogens.

# Outlook

This thesis presents the work, which identifies Glidobactin C as specific inhibitor of β2/β5 subunits of the proteasome. Previous research suggests simultaneous inhibition of both β2 and β5 subunits in solid tumors leads to a decrease in tumor growth.[26] Thus, Glidobactin C makes an ideal inhibitor and promising anti-cancer drug candidate against solid tumors.

Another aspect to be studied is the structure-activity relationship of the syrbactins core and its inhibition pattern on the different subunits of the proteasome. Based on my results, it is clear that minor differences in the core structure of the syrbactins shows differential inhibition pattern in the proteasome. Using combinatorial synthetic chemistry to synthesize non-canonical syrbactins core structure and testing the inhibition pattern would provide important information about the proteasome, and its potential role in cancer development.

In the same vein, it is equally important to study the effect on the syrbactins tail moiety on the cell permeability and efficacy. Modulation of cell permeability of syrbactins is also important, if the molecule is considered as a potential anti-cancer molecule.

Lastly, the competitive metabolite profiling of natural products as described in this thesis, provides a good alternative to traditional natural product discovery. The strategy is scalable and can be easily implemented to other clinically important target proteins, which need to be studied in more detail with chemical biology approaches as well as proteomics.

# Materials and Methods

## General methods

All solvents, culture media and chemical reagents were purchased either from Sigma Aldrich, VWR or Carl Roth. NMR spectra were measured with a Bruker Avance-III 400 MHz and Bruker Avance-III 600 MHz NMR spectrometer at ambient temperature. The data obtained were processed and analyzed with MestReNova software. Mass spectrometry data were obtained on an ESI-Orbitrap (Thermo Scientific, LTQ Orbitrap Velos) via direct injection, and analyzed with Xcalibur (Thermo Scientific) software.

Preparative scale PeqLab gel electrophoresis systems were used for SDS-PAGE based protein electrophoresis. The analysis and image capture of the fluorescence and Coomassie Brilliant Blue stained gels was performed with a Fusion-FX7 Advanced (by?) Vilber Lourmat (Eberhardzell, Germany) using the software FusionCapt Advance.

## Microbial Strains

Glycerol (15%) based bacterial cryostocks stored at -80°C were used to inoculate culture media for making starter cultures in 13 mL polypropylene tubes (Sarstedt) with appropriate shaking and temperature. *Pseudomonas syringae pv. syringae* B301D-R harboring the plasmid construct pOEAC for overproduction of SylA was a gift from Prof. Dr. Robert Dudler at University of Zurich. Unclassified strain, DSM 7029 was obtained from DSMZ microbial collection.

## Overproduction and isolation of syringolin A from Pseudomonas syringae

The Syringolin A production medium $SRM_{AF}$ was prepared as described previously.[23] Two-day-old starter cultures of *Pseudomonas syringae* pv. *syringae* B301D-R in 50 mL of medium supplemented with 10 µg/mL tetracycline were used to inoculate 5 L $SRM_{AF}$ medium in Erlenmeyer flasks. Cultures for Syringolin A production were grown for 10 days at 28°C under shaking at 160 rpm. Syringolin A production was monitored by analytical HPLC with a C18 RP, 250 x 4.6 mm, 7 µm column from Dr. Maisch HPLC GmbH at 2 mL/min flow rate with 20% isocratic acetonitrile in water mixture containing 0.01% formic acid with an elution time at 15.5 min. After 10 days of growth, the culture

was centrifuged at 9000 rpm for 10 min to pellet down the cells, and the supernatant was sterilized by passing through 0.22 µm sterile filters. Amberlite XAD-16N beads (20-60 mesh, Sigma-Aldrich) were washed before use by stirring overnight in deionized water at room temperature. A dry weight of 10 g of Amberlite XAD-16N was used per 1 L of $SRM_{AF}$ medium. The beads were added and allowed to absorb metabolites for 4 h at room temperature while stirring. The beads were then filtered out and washed twice with distilled water to remove salts and media components and washed with 20% methanol. The crude metabolites from the beads were finally eluted overnight with 80% isopropanol, and the eluate was dried under reduced vacuum to give crude Syringolin A containing extract. Preparative HPLC was performed with a C18AQ RP 250 x 20 mm, 10 µm column from Dr. Maisch HPLC GmbH with a flow rate of 15 mL/min in an isocratic run with 20% acetonitrile in water. Detector scanning was set at scan from 200 – 800 nm. Syringolin A was eluted and subsequently collected at 25 min in three fractions that were combined to give 9 mg of pure Syringolin A as white solid as shown in **Figure 5A**. HR-MS and NMR were performed to confirm the purity as shown in **Figure 25** and **26**.

## Click Chemistry

Click Chemistry (CC) was performed with 44 µL of sample volume by subsequent addition of 1 µL of 0.65 mM 5-carboxytetramethylrhodamine azide (5-TAMRA azide; Baseclick, Munich) stock in DMSO (prepared from a 193 mM stock in MeOH), 1 µL of freshly prepared 52 mM tris(2-carboxyethyl)phosphine hydrochloride solution in water, 3 µL of 1.66 µM tris[(1-benzyl-1H-1,2,3-triazol-4-yl)methyl]amine (TBTA) and 1 µL of 50 mM CuSO4. The reagents were mixed well by vortexing and incubated at room temperature for 1 hour and quenched by addition of 50 µL of 2x SDS loading buffer (63 mM Tris-HCl, 10% (v/v) glycerol, 2% (w/v) SDS, 0.0025% (w/v) bromophenol blue, 10% (v/v) β-mercaptoethanol; in water).

## Standard labelling assay

Purified 20S proteasome (5 µg) in activation buffer (Tris-HCl 50 mM, KCl 25 mM, NaCl 10 mM, MgCl2, 0.1 mM EDTA, 1 mM, SDS 0.02% and 1 mM DTT) was used for the standard labelling assay. Hereby, 1 µL of syringolin A probe was added along with proteasome in freshly prepared in activation buffer to volume of 44 µL. The reaction

mixture was incubated for 1 hour at 37°C at 500 rpm in 1.5 mL Eppendorf tubes. The reaction vial was then used for click chemistry, quenched with SDS-loading buffer and stored at -20°C until SDS PAGE was performed.

## Syringolin A probe synthesis

To a solution of syringolin A (9.9 µmol, 4.9 mg) in 150 µL of 1:1 DMF/DMSO was added HBTU (1.5 equiv., 14.8 µmol, 5.6 mg) at 0°C followed by but-3-yn-1-amine (2 equiv., 19.9 µmol, 1.63 µL) and DIPEA (5 equiv., 49.6 µmol, 8.64 µL) was added to the reaction. The ice bath was removed and reaction was stirred for 72 hours at room temperature. Another portion of HBTU (1.5 equiv., 14.8 µmol, 5.6 mg) was added and stirred for additional 24 hours. The reaction mixture was then lyophilized and 50% acetonitrile in water was added to the reaction, resulting in a white suspension. The suspension was centrifuged to collect the white precipitate. The supernatant was discarded. The solid was dried by lyophilization and the product (SylP) was confirmed by HR-MS and NMR (**Figure 25** and **27**) with a yield of 57%.

## Competitive labelling assay

Purified 20S proteasome (5 µg) in activation buffer (Tris-HCl 50 mM, KCl 25 mM, NaCl 10 mM, MgCl2, 0.1 mM EDTA, 1 mM, SDS 0.02% and 1 mM DTT) was used for the competitive labelling assay. Metabolite extracts or fractions of unknown metabolite or characterized metabolite stock solution (1 µL) in DMSO were added to 43 µL of proteasome in freshly prepared in activation buffer. The reaction mixture was incubated for 1 hour at 37°C at 500 rpm in Eppendorf tubes. Subsequently, 1 µL of syringolin A probe was added to final concentration of 1 µM and incubated for 1 hour at 37°C at 500 rpm. The sample was then subjected to click chemistry, quenched with SDS-loading buffer and stored at -20°C until SDS PAGE was performed. Representative fluorescence labelled lanes is shown in **Figure 12**.

## Extraction and purification of Glidobactin A, Luminmycin A and Glidobactin C

Unclassified strain DSM 7029 (DSMZ microbial collection) was grown in SOB (super optimal broth, 2% w/v tryptone, 0.5% w/v yeast extract, 10 mM NaCl, 2.5 mM KCl, 10 mM MgCl2, 10 mM MgSO4) medium. The initial culture was grown at 30°C at 180 rpm

in a shaking incubator for 2 days. 50 mL of 2-day-old culture was used to inoculate production medium (2% soluble starch, 3% soy peptone, 0.3% $MgSO_4 \cdot 7H_2O$, 1% $CaCO_3$, adjusted to pH 7.0 before sterilization). The production medium culture was grown for 7 days at 30 °C at 180 rpm. The downstream processing was carried out by pelleting the cells in a centrifuge at 10000 rpm for 10 min at room temperature. The clear culture supernatant was extracted twice with equal volumes of ethyl acetate. The solvent from the filtered organic fraction was evaporated under vacuum. The crude extract was subjected to preparative RP-HPLC with a Reprosil C18 amide column (250 mm x 20 mm, 10 µm): solvent A = water + 0.01% formic acid; solvent B = acetonitrile + 0.01% formic acid. Gradient: T0min: 5% B (isocratic), $T_{15min}$: 5% B (linear gradient) $T_{45min}$: 95% (isocratic), $T_{60min}$: 95% B. The retention time for Glidobactin A was 37 min, for Luminmycin A 41 min and for Glidobactin C 42 min. The crude fractions were purified to homogeneity using semi-preparative reverse phase HPLC with a Reprosil C18 amide column (250 mm x 10 mm, 10 µm): solvent A = water + 0.01% formic acid; solvent B = acetonitrile + 0.01% formic acid. Gradient: T0min: 50% B (isocratic), T35min: 50% B (linear gradient) T40min: 95% (isocratic), T47min: 95% B. Elution time for Glidobactin A was 16 min, for Luminmycin A was 25 min and for Glidobactin C was 39 min.

## Bradford Assay

The protein concentration of the proteasome was determined with the Bradford assay, using the Thermo Fisher Pierce Coomassie (Bradford) Protein Assay Kit. The absorption at 595 nm is measured to determine protein concentration of the sample. A dilution series of bovine serum albumin (BSA) was prepared. 250 µL of Coomassie assay reagent were added to 5 µL of each standard or the proteasome solution and then read in a transparent Sarstaedt 96 well plate. Samples were incubated at room temperature for 10 min before the absorption was measured in an infinite M200 pro plate reader (TECAN, Männedorf). The measured absorptions of the dilutions were plotted against their protein concentration, yielding a standard curve. Concentrations of the proteasome solutions were calculated with the aid of this standard curve.

## Preparation of Polyacrylamide Gels

To make the SDS-PAGE gels, 3.75% stacking gel and 10% separation gel was used. Each component was thoroughly mixed with a vortex. Rotiphorese Gel 30 (Carl Roth, Karlsruhe, Germany), a stabilized 30 % aqueous solution of 37.5:1 acrylamide and bisacrylamide was used. For one gel of the large Peqlab gel system, the 1.5-fold amount of separation gel and the 1.25-fold amount of stacking gel were prepared. Polymerized gels were either run instantly or kept damp and stored at 4 °C.

## Analysis of Proteins by means of SDS-PAGE

In each case the pockets of the SDS-PAGE gels were loaded with 50 µL of samples including 2 × SDS-PAGE loading buffer or 10 µL of Roti-Mark BI-PINK (Carl Roth, Karlsruhe, Germany), respectively. The gels were run in 1 × SDS-PAGE running buffer with a maximum voltage of 300 V. Initially, the constant current was set to 55 mA to prevent formation of uneven bands until the bands passed the stacking gel, followed by a current change to 75 mA after one hour. The SDS-PAGE gels were monitored by in-gel Rhodamine azide fluorescence detection using a FUSION-FX7 Advance with an EPI-UV/Blue and SUPER-BRIGHT illumination system, equipped with a 4.2/10 Mio Pixel CCD-Camera, a Fusion SPECTRA LED EPI Illuminator Device for excitation of fluorescent dyes and an F595 Y3 camera filter for emission maxima >550 nm (VWR) with an absorption wavelength of 546 nm and an emission wavelength of 579 nm. The visualization of sufficient protein loading was done by the Coomassie blue staining, using the prepared Coomassie staining solution overnight, with subsequent de-staining solution over several days or InstantBlue (expedeon, Heidelberg, Germany) overnight. Staining and de-staining was carried out on a platform shaker. The stained gels were scanned with the FUSION-FX7 Advance conversion screen method.

## Nuclear Magnetic Resonance

Proton nuclear magnetic resonance (1H NMR) spectra were recorded on a Bruker Avance III 600 spectrometer. NMR data were processed and analysed with MestReNova software. 1H NMR spectra were referenced to the residual proton signal of the deuterated solvent and are reported as follows: chemical shift δ in ppm, multiplicity, coupling constant in Hz and integration. Multiplicities are given with s – singulet, d –

doublet, t – triplet, q – quartet, quin - quintet and m – multiplet or combinations thereof. Chemical shifts (δ) are given in parts per million (ppm) relative to the residual solvent signals of DMSO-d6 $^{\delta}$H = 2.50 ppm and $^{\delta}$C = 39.52 ppm.

# Annex

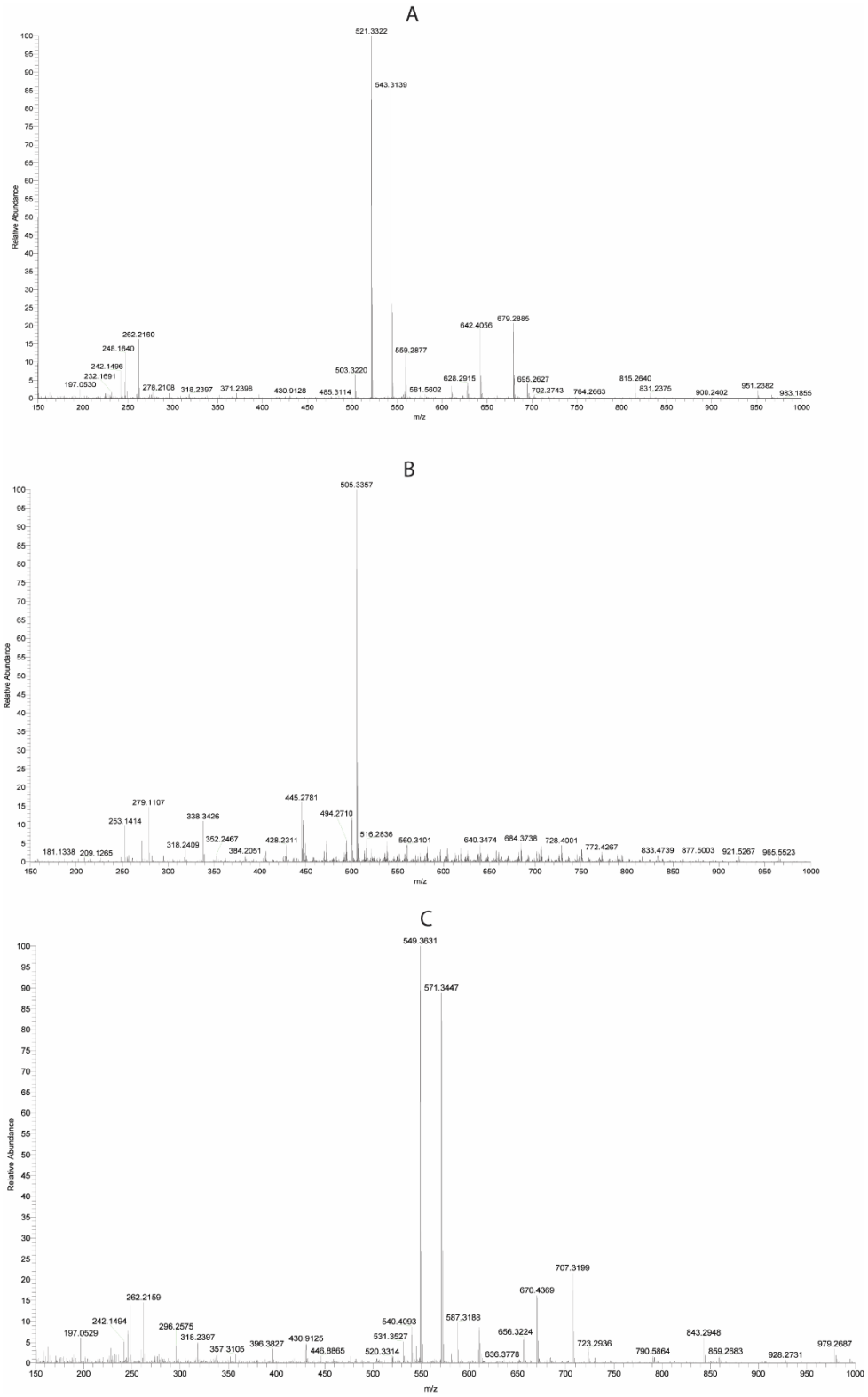


**Figure 25**: High resolution Mass spectrum of GlbA (A), LumA (B), and GlbC (C).

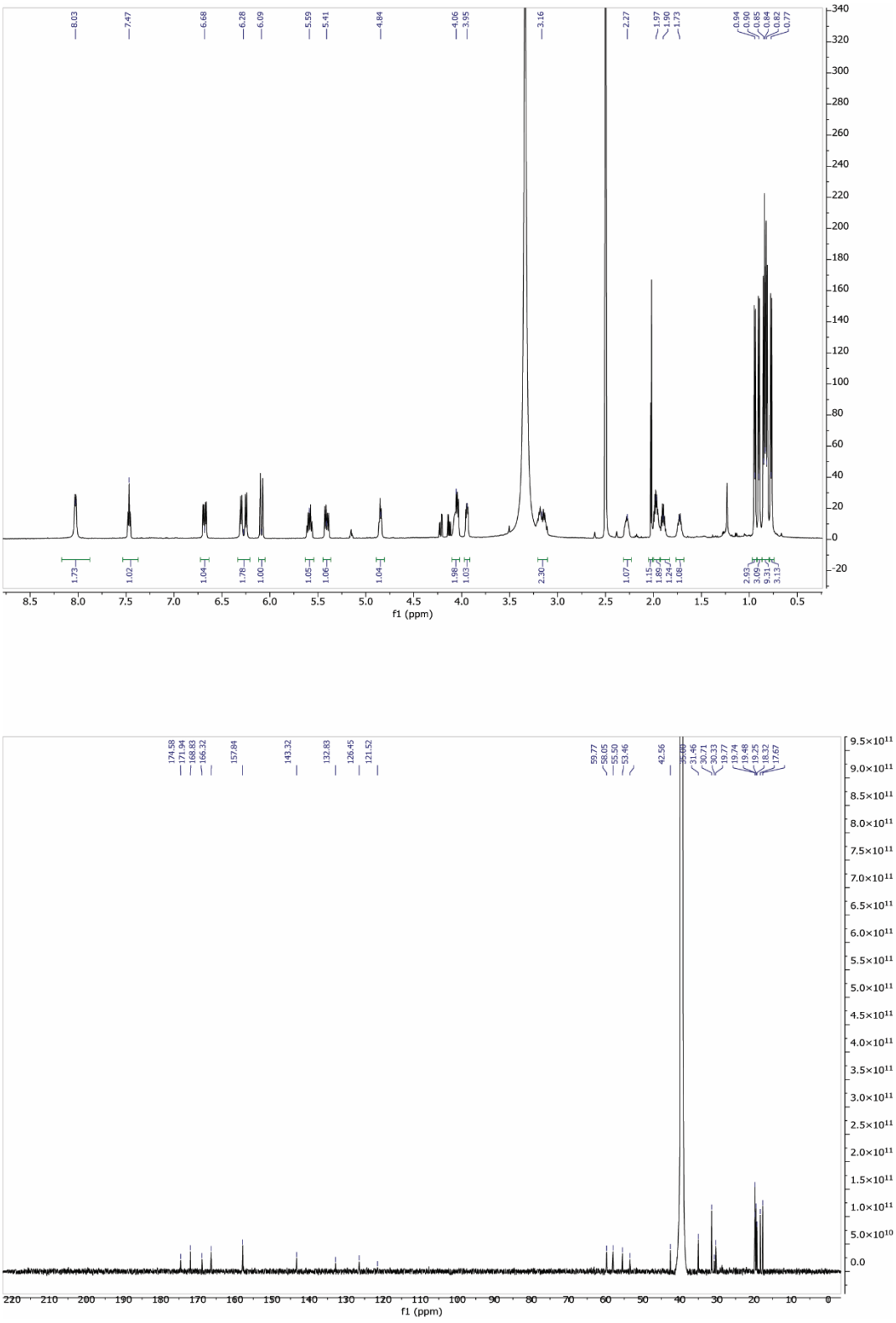


**Figure 26**: NMR of $^{1}H$ and $^{13}C$ for SylA

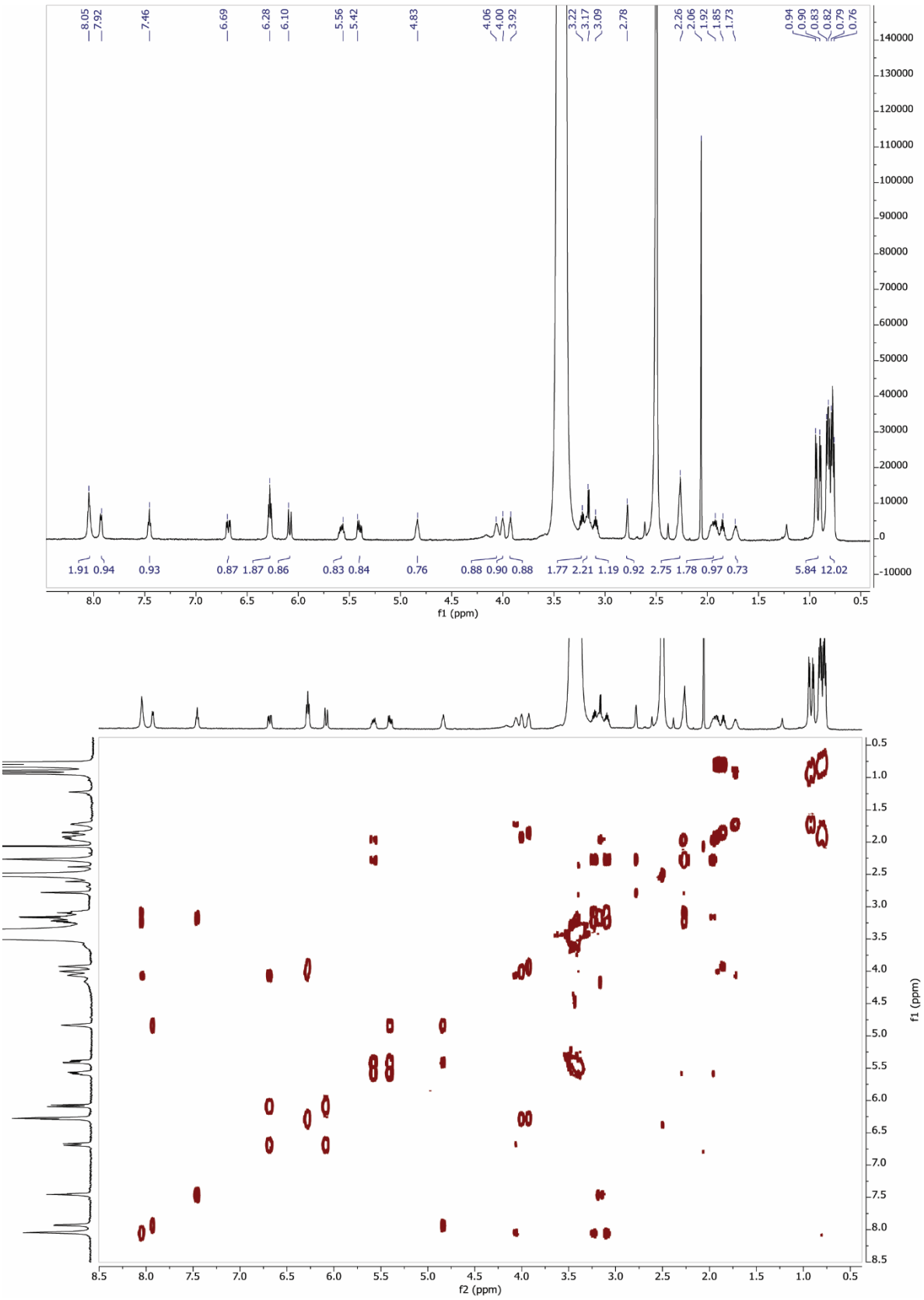
8.05
7.92
7.46
6.69
6.28
6.10
5.56
5.42
4.83
4.06
4.00
3.92
3.22
3.17
3.09
2.78
2.26
2.06
1.92
1.85
1.73
0.94
0.90
0.83
0.82
0.79
0.76
1.91 0.94
0.93
0.87 1.87 0.86
0.83 0.84
0.76
0.88 0.90 0.88
1.77 2.21 1.19 0.92 2.75 1.78 0.97 0.73
5.84 12.02
f1 (ppm)
f2 (ppm)
f1 (ppm)

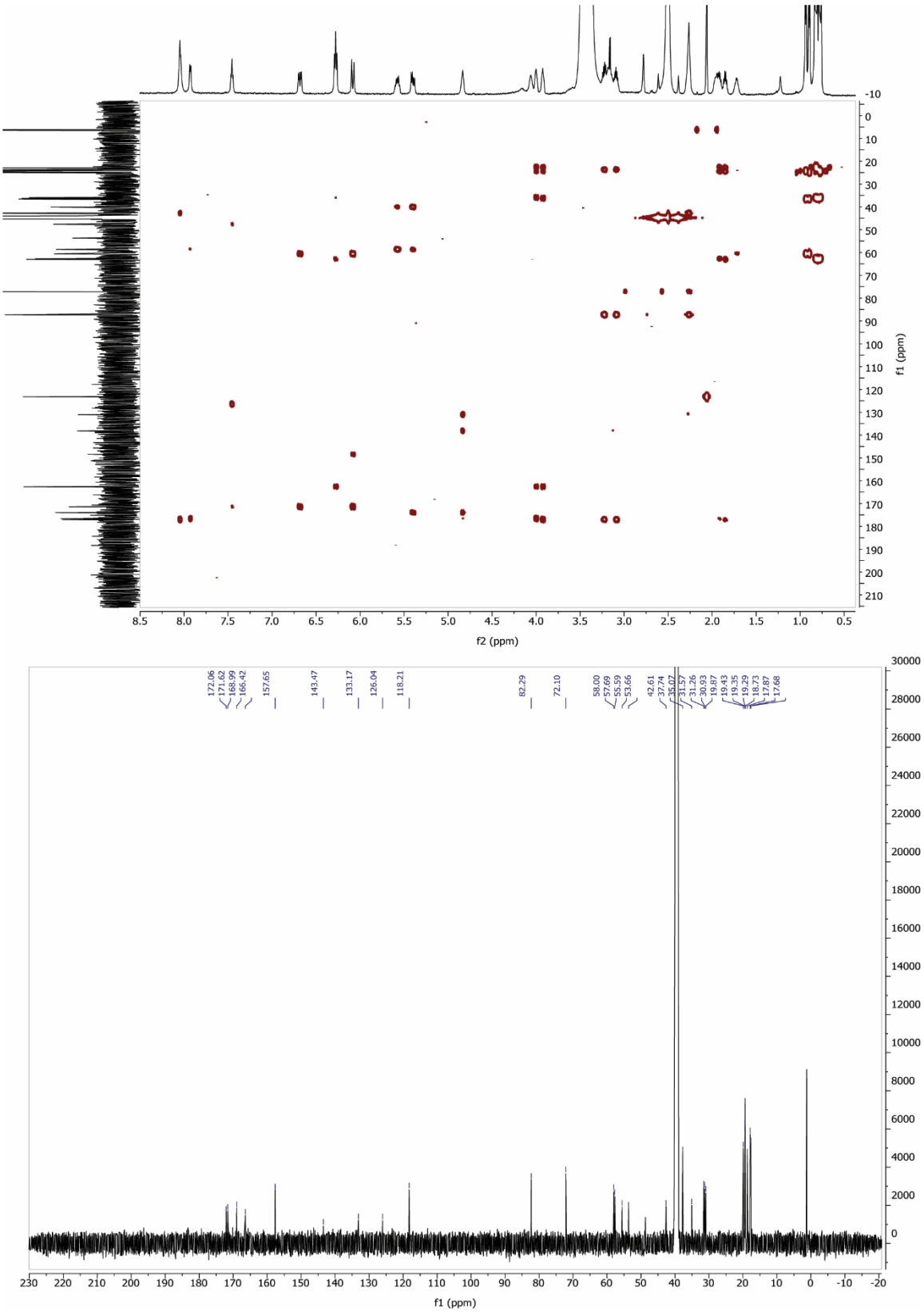


**Figure 27**: NMR of $^{1}H$, $^{1}H$-$^{1}H$ COSY, $^{1}H$-$^{13}C$ HMBC and $^{13}C$ for SylP

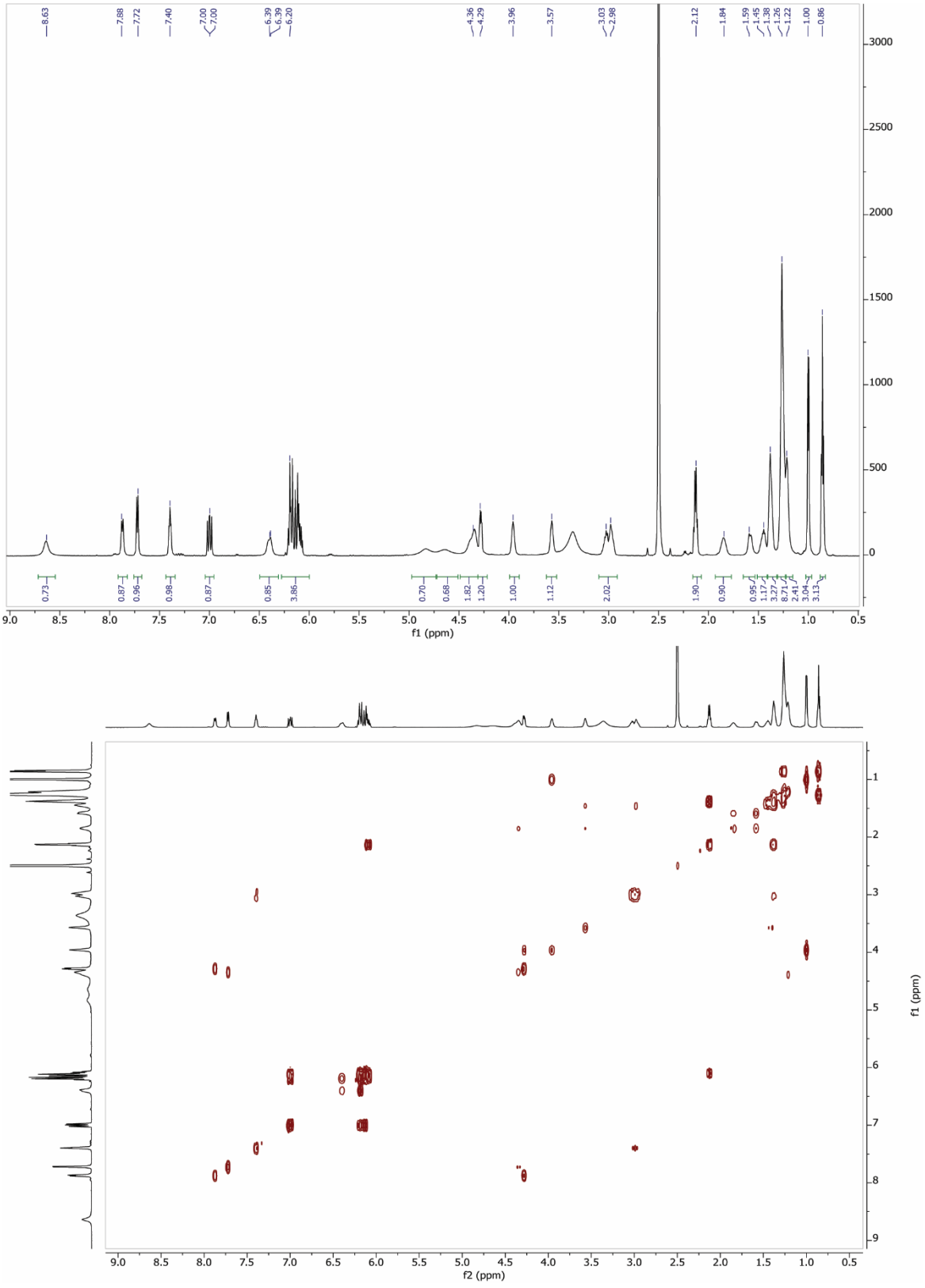
8.63
7.88
7.72
7.40
7.00
7.00
6.39
6.39
6.20
4.36
4.29
3.96
3.57
3.03
2.98
2.12
1.84
1.59
1.45
1.38
1.26
1.22
1.00
0.86
0.73
0.87
0.96
0.98
0.87
0.85
3.86
0.70
0.68
1.82
1.20
1.00
1.12
2.02
1.90
0.90
0.95
1.17
3.27
8.71
2.41
3.04
3.13
f1 (ppm)
f2 (ppm)
f1 (ppm)

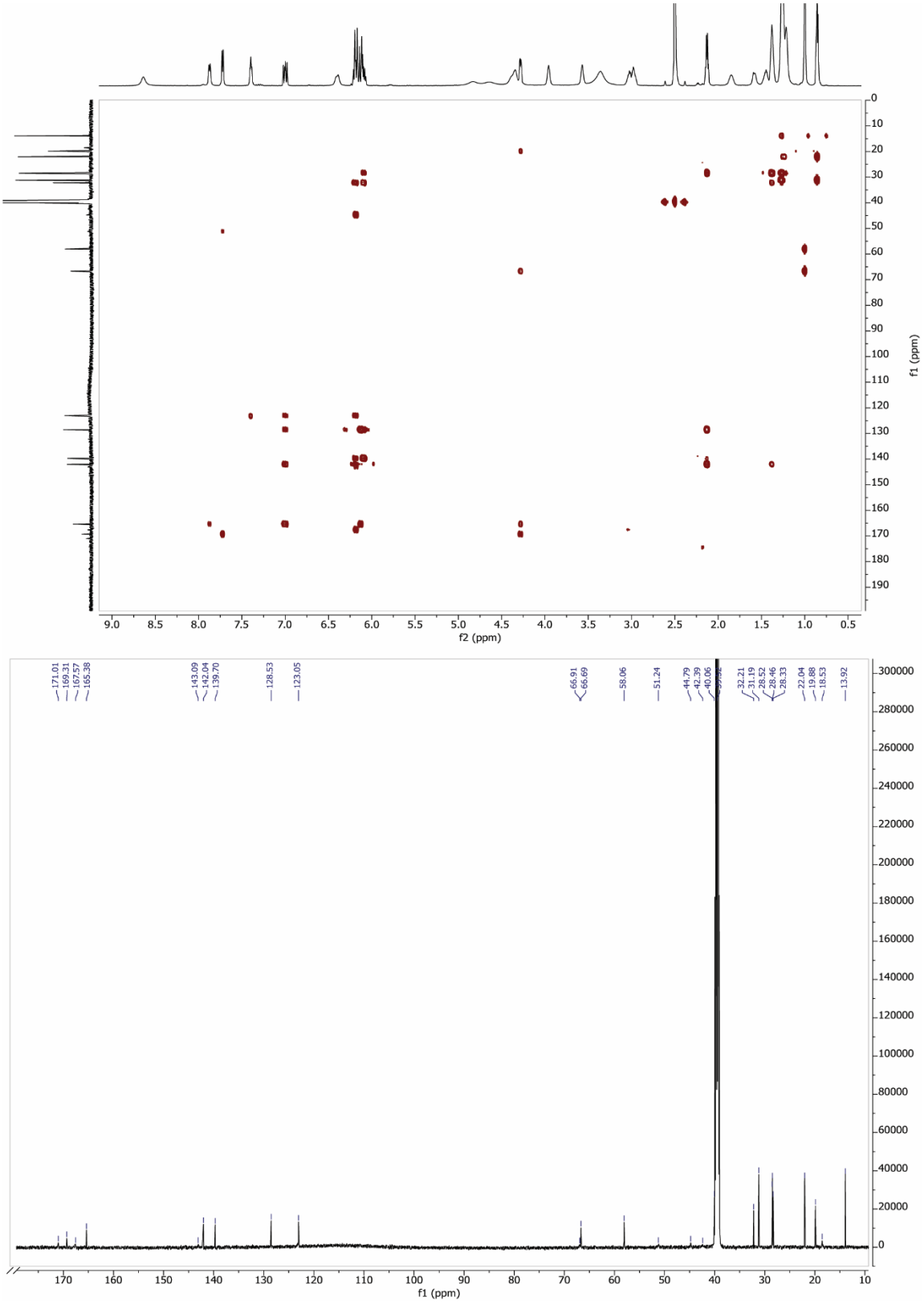


**Figure 28**: NMR of $^{1}H$, $^{1}H$-$^{1}H$ COSY, $^{1}H$-$^{13}C$ HMBC and $^{13}C$ for GlbA

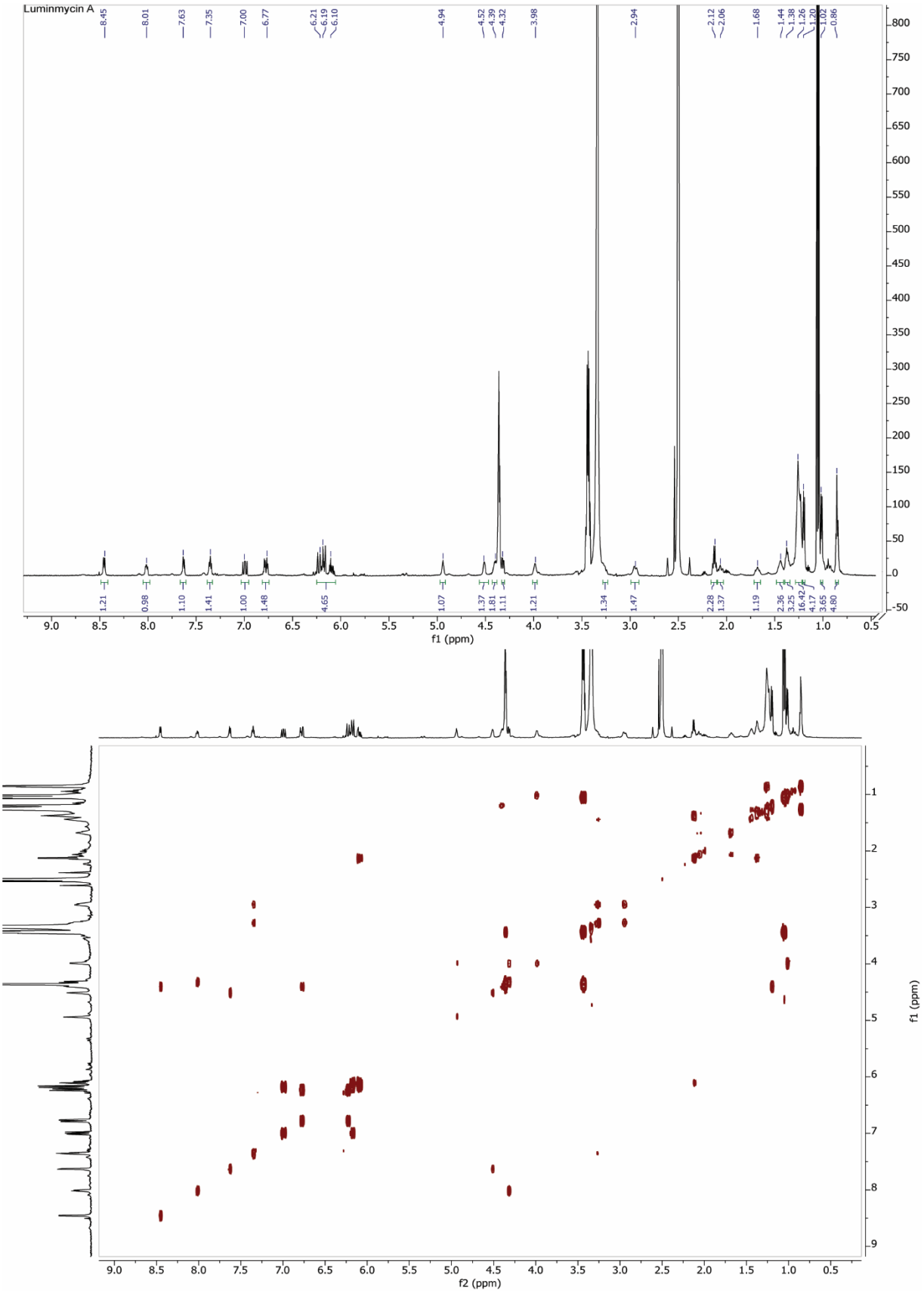
Luminmycin A
8.45
8.01
7.63
7.35
7.00
6.77
6.21
6.19
6.10
4.94
4.52
4.39
4.32
3.98
2.94
2.12
2.06
1.68
1.44
1.38
1.26
1.20
1.02
0.86
1.21
0.98
1.10
1.41
1.00
1.48
4.65
1.07
1.37
1.81
1.11
1.21
1.34
1.47
2.28
1.37
1.19
2.36
3.25
16.42
4.17
3.65
4.80
f1 (ppm)
f2 (ppm)

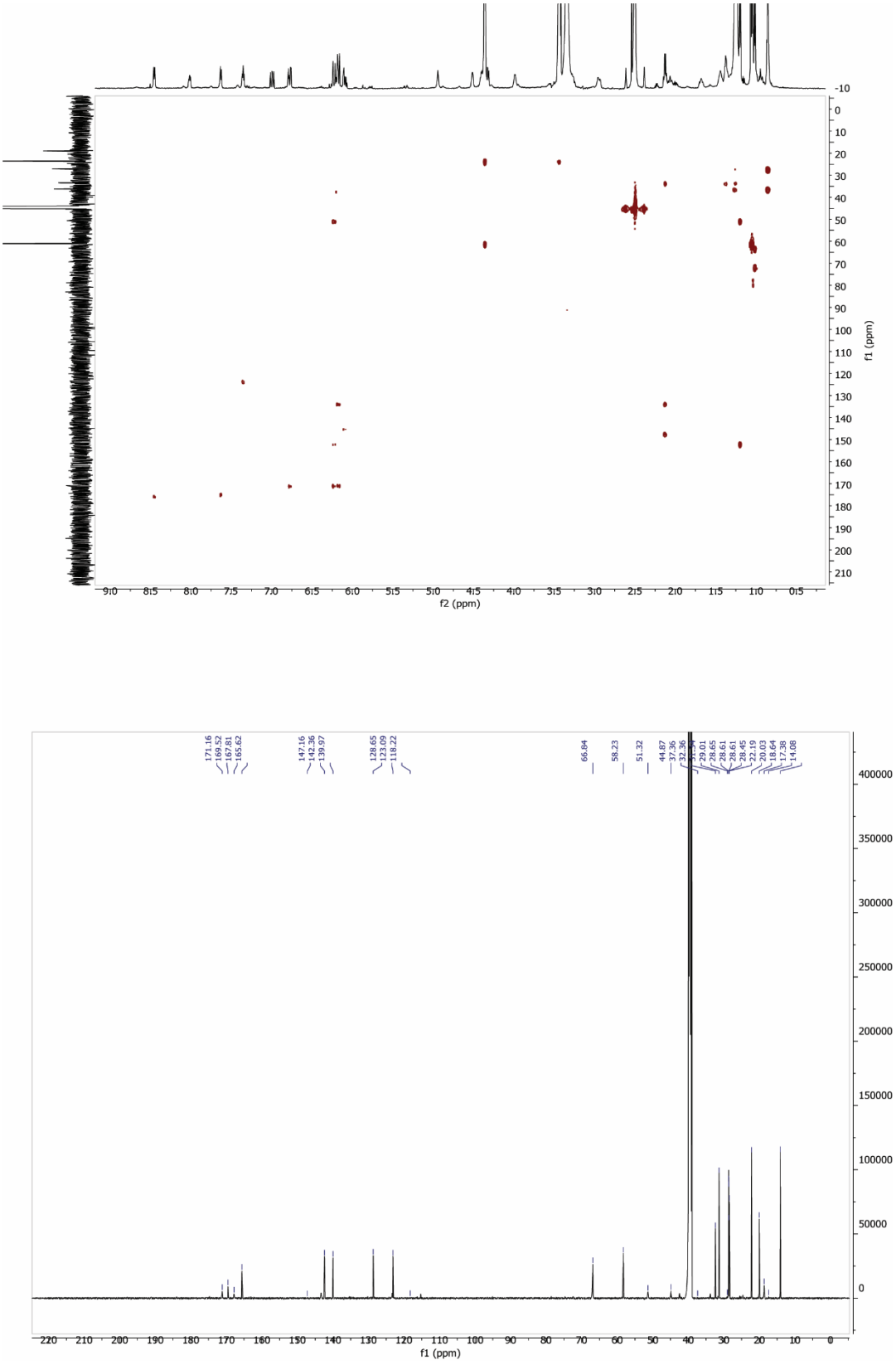


**Figure 29**: NMR of $^{1}H$, $^{1}H$-$^{1}H$ COSY, $^{1}H$-$^{13}C$ HMBC and $^{13}C$ for LumA

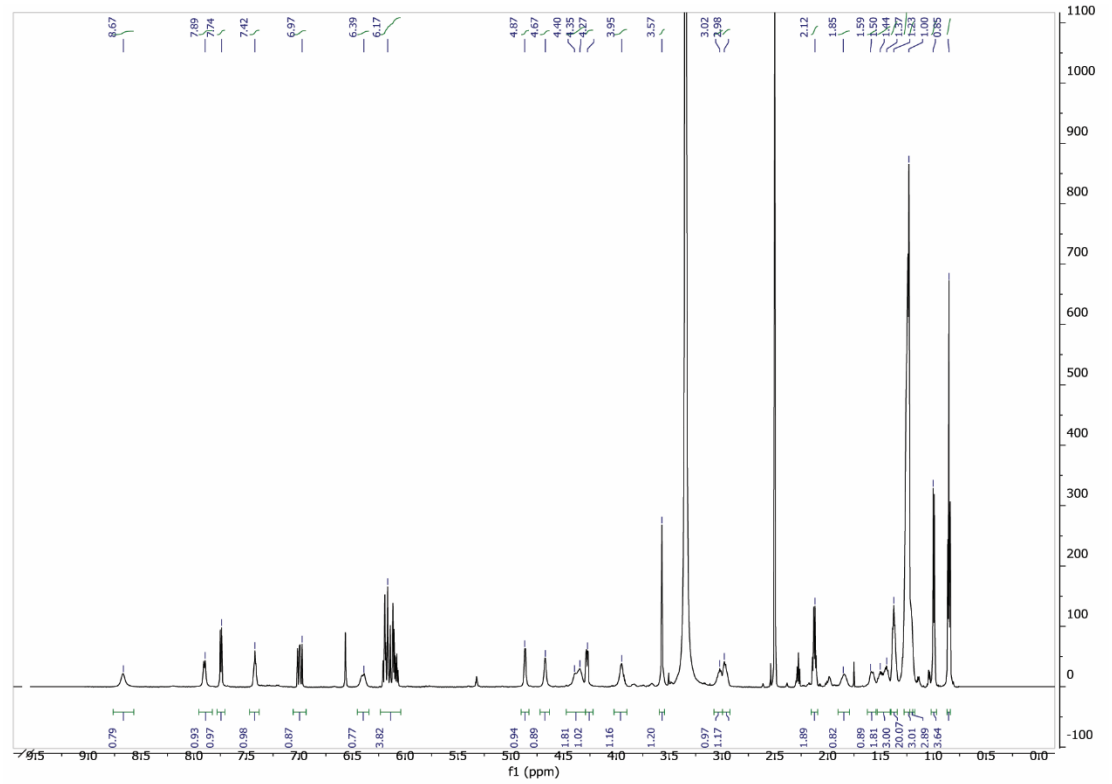
f1 (ppm)

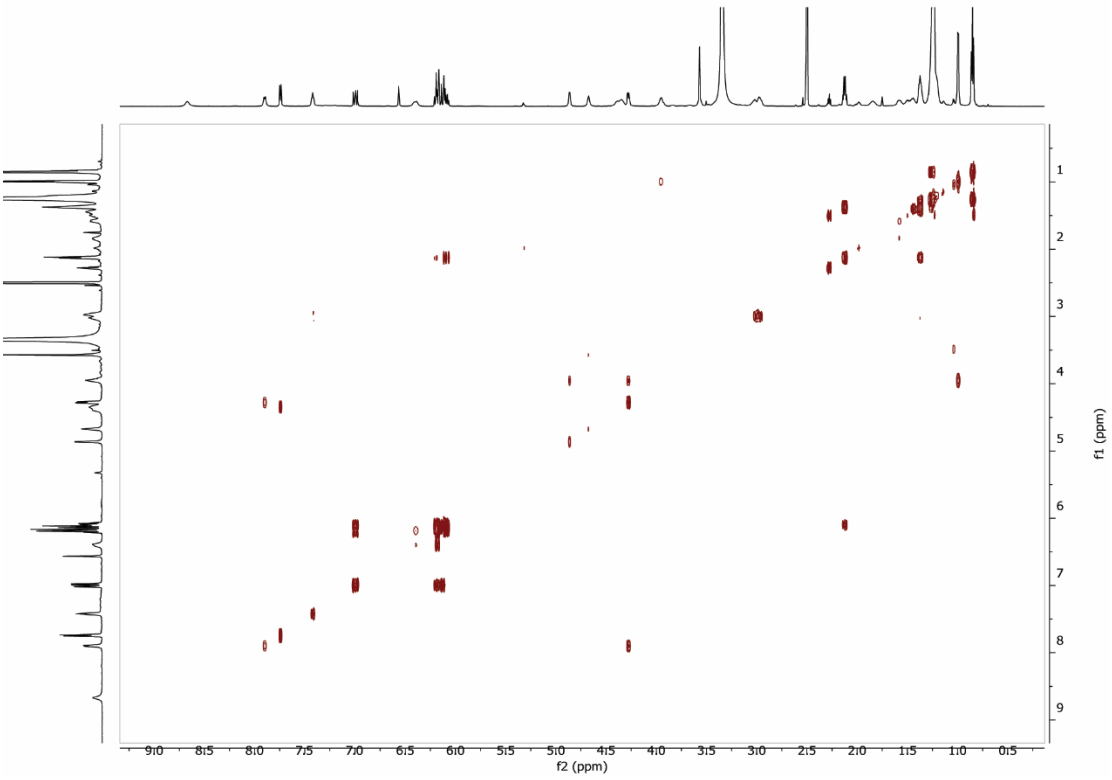
f2 (ppm)
f1 (ppm)

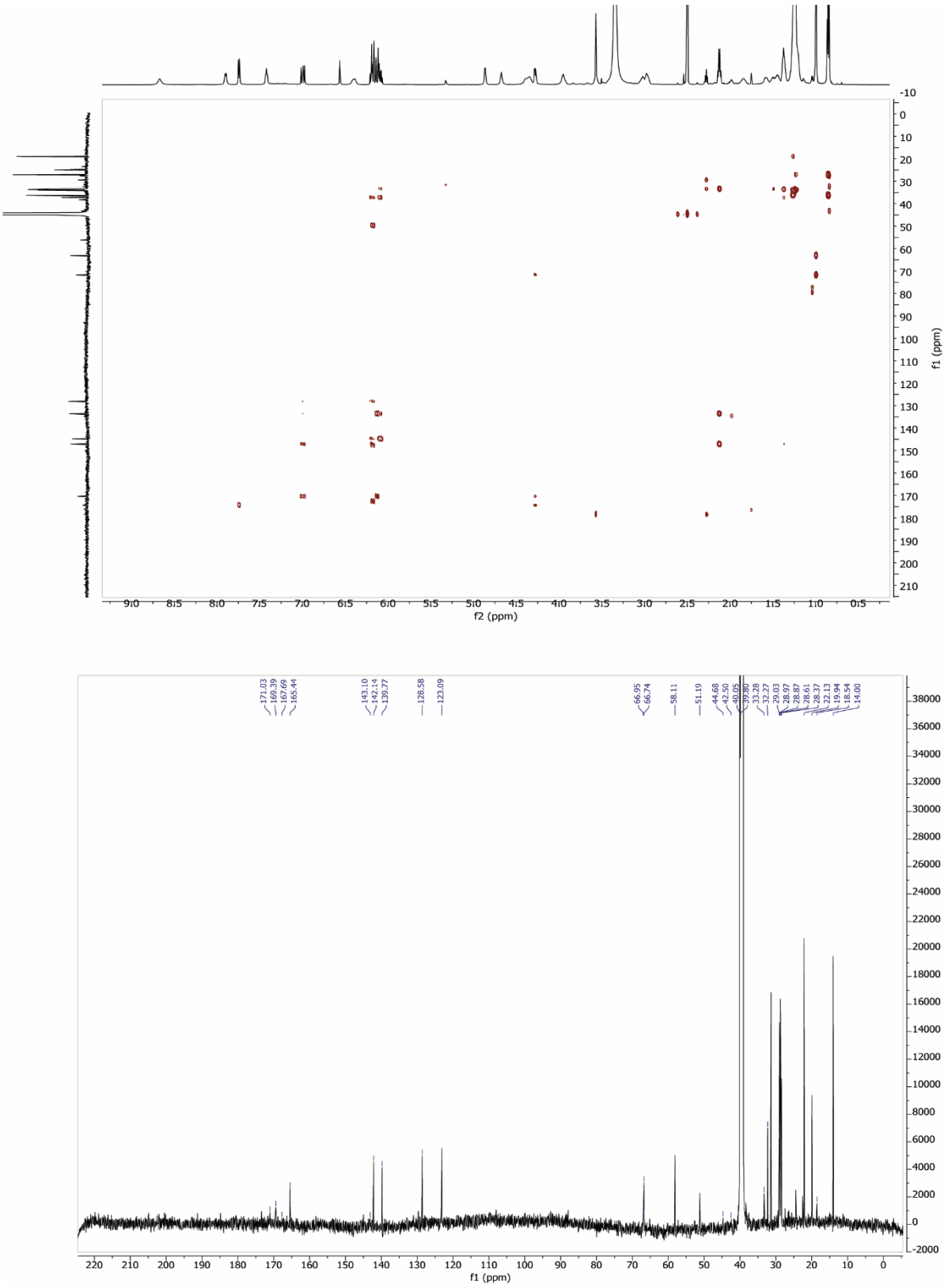


**Figure 30**: NMR of $^{1}H$, $^{1}H$-$^{1}H$ COSY, $^{1}H$-$^{13}C$ HMBC and $^{13}C$ for GlbC

# List of figures and tables

# Author‘s publication

Parts in this thesis are taken from author’s publication as cited below:

Competitive Metabolite Profiling of Natural Products Reveals Subunit Specific Inhibitors of the 20S Proteasome

Atul Pawar, Michael Basler, Heike Goebel, Gerardo Omar Alvarez Salinas, Marcus Groettrup, and Thomas Böttcher

*ACS Central Science* **2020** *6* (2), 241-246

DOI: 10.1021/acscentsci.9b01170

# References


[1] D. H. Williams, M. J. Stone, P. R. Hauck, S. K. Rahman, *J. Nat. Prod.* **1989**, *52*, 1189–1208.

[2] D. J. Newman, G. M. Cragg, *J. Nat. Prod.* **2020**, *83*, 770–803.

[3] K. Tanaka, *Proc. Japan Acad. Ser. B Phys. Biol. Sci.* **2009**, *85*, 12–36.

[4] M. Groll, L. Ditzel, J. Lowe, D. Stock, M. Bochtler, H. Bartunik, R. Huber, *Nature* **1997**, *386*, 463–471.

[5] A. F. Kisselev, W. A. Van Der Linden, H. S. Overkleeft, *Chem. Biol.* **2012**, *19*, 99–115.

[6] I. Momose, Y. Umezawa, S. Hirosawa, M. Iijima, H. Iinuma, D. Ikeda, *Biosci. Biotechnol. Biochem.* **2005**, *69*, 1733–1742.

[7] G. Lin, D. Li, T. Chidawanyika, C. Nathan, H. Li, *Arch. Biochem. Biophys.* **2010**, *501*, 214–220.

[8] M. Groll, V. S. Korotkov, E. M. Huber, A. de Meijere, A. Ludwig, *Angew. Chemie Int. Ed.* **2015**, *201502931*, n/a-n/a.

[9] R. H. Feling, G. O. Buchanan, T. J. Mincer, C. A. Kauffman, P. R. Jensen, W. Fenical, *Angew. Chemie - Int. Ed.* **2003**, *42*, 355–357.

[10] L. Meng, R. Mohan, B. H. B. Kwok, M. Elofsson, N. Sin, C. M. Crews, *Proc. Natl. Acad. Sci. U. S. A.* **1999**, *96*, 10403–10408.

[11] J. Zettler, F. Zubeil, A. Kulik, S. Grond, L. Kaysser, *ChemBioChem* **2016**, *17*, 792–798.

[12] J. Clerc, B. I. Florea, M. Kraus, M. Groll, R. Huber, A. S. Bachmann, R. Dudler, C. Driessen, H. S. Overkleeft, M. Kaiser, *ChemBioChem* **2009**, *10*, 2638–2643.

[13] C. Ramel, M. Tobler, M. Meyer, L. Bigler, M.-O. Ebert, B. Schellenberg, R. Dudler, *BMC Biochem.* **2009**, *10*, 26.

[14] D. Krahn, C. Ottmann, M. Kaiser, *Nat. Prod. Rep.* **2011**, *28*, 1854–1867.

[15] J. A. Titus, C. A. Roundy, *J. Ind. Microbiol.* **1990**, *6*, 215–218.

[16] S. M. S. and J. O. Aleksej Krunic, Armelle Vallat†, Shunyan Mo, Daniel D. Lantvit, *Bone* **2012**, *23*, 1–7.

[17] I. Nickeleit, S. Zender, F. Sasse, R. Geffers, G. Brandes, I. Sörensen, H. Steinmetz, S. Kubicka, T. Carlomagno, D. Menche, et al., *Cancer Cell* **2008**, *14*, 23–35.

[18] B. F. Cravatt, A. T. Wright, J. W. Kozarich, *Annu. Rev. Biochem.* **2008**, *77*, 383–414.

[19] I. Staub, S. a. Sieber, *J. Am. Chem. Soc.* **2009**, *131*, 6271–6276.

[20] H. C. Kolb, M. G. Finn, K. B. Sharpless, *Angew. Chem. Int. Ed. Engl.* **2001**, *40*, 2004–2021.

[21] S. Zweerink, V. Kallnik, S. Ninck, S. Nickel, J. Verheyen, M. Blum, A. Wagner, I. Feldmann, A. Sickmann, S. V. Albers, et al., *Nat. Commun.* **2017**, *8*, DOI 10.1038/ncomms15352.

[22] A. E. Speers, B. F. Cravatt, *Curr. Protoc. Chem. Biol.* **2009**, *1*, 29–41.

[23] C. Ramel, N. Baechler, M. Hildbrand, M. Meyer, D. Schädeli, R. Dudler, *Mol. Plant. Microbe. Interact.* **2012**, *25*, 1198–208.

[24] A. Pawar, M. Basler, H. Goebel, G. O. Alvarez Salinas, M. Groettrup, T. Böttcher, *ACS Cent. Sci.* **2020**, DOI 10.1021/acscentsci.9b01170.

[25] R. Oerlemans, C. R. Berkers, Y. G. Assaraf, G. L. Scheffer, G. J. Peters, S. E. Verbrugge, J. Cloos, J. Slootstra, R. H. Meloen, R. H. Shoemaker, et al., *Invest. New Drugs* **2018**, 1–13.

[26] S. Downey-Kopyscinski, E. W. Daily, M. Gautier, A. Bhatt, B. I. Florea, C. S. Mitsiades, P. G. Richardson, C. Driessen, H. S. Overkleeft, A. F. Kisselev, *Blood Adv.* **2018**, *2*, 2443–2451.

[27] M. B. and M. Groettrup, *Methods Mol. Biol.* **2012**, *832*, 423–432.